

# Working Paper

## Adaptive Robust Optimization for European Electricity System Planning Considering Regional Dunkelflaute Events

\* Maximilian Bernecker (BTU Cottbus-Senftenberg), [maximilian.bernecker@b-tu.de](mailto:maximilian.bernecker@b-tu.de)

Smaranda Sgarciu (BTU Cottbus-Senftenberg), [smaranda.sgarciu@b-tu.de](mailto:smaranda.sgarciu@b-tu.de)

Xiaoming Kan (Chalmers University of Technology) [kanx@chalmers.se](mailto:kanx@chalmers.se)

Mehrnaz Anvari (Fraunhofer) (Fraunhofer SCAI), [mehrnaz.anvari@uni-oldenburg.de](mailto:mehrnaz.anvari@uni-oldenburg.de)

Igor Riepin (TU Berlin), [igor.riepin@tu-berlin.de](mailto:igor.riepin@tu-berlin.de)

Felix Müsgens (BTU Cottbus-Senftenberg), [felix.muesgens@b-tu.de](mailto:felix.muesgens@b-tu.de)

\* Corresponding author.

*E-mail address:* [maximilian.bernecker@b-tu.de](mailto:maximilian.bernecker@b-tu.de) (M. Bernecker)

**Keywords:** Renewable electricity system, Extreme weather events, Adaptive robust optimization, Long-term planning, Power generation, Transmission expansion

## Nomenclature

### Indices

t	Time steps
n	Nodes
l	Transmission lines, AC and DC
r	Solar & wind generation units
c	Conventional (conv.) generation units
b	Battery storage unit
h	Hydrogen storage unit
ror	Hydro run of river plant
rsv	Hydro reservoir plant
psp	Hydro pumping storage plant
g	Geographical weather region

### Sets

$r(l)$	Receiving node of transmission line
$s(l)$	Sending node of transmission line
$AC(l)$	Alternating current Transmission line
$DC(l)$	Direct current Transmission line
$\Phi_n^R$	Solar, wind power plants located at node n
$\Phi_n^P$	Conventional power plants located at node n
$\Phi_n^B$	Battery storage units located at node n
$\Phi_n^H$	Hydrogen storage units located at node n
$\Phi_n^{ROR}$	Run of river plants located at node n
$\Phi_n^{PSP}$	Pumping storage plants located at node n
$\Phi_n^{RSV}$	Hydro reservoir plant located at node n
$pv(r)$	Solar PV power plants
$wind(r)$	Wind turbines
$ref(n)$	Slack or reference node

### Scalars

$f^{L1}$	Percentage of flexible demand level 1
$f^{L2}$	Percentage of flexible demand level 2
$f^{L3}$	Percentage of flexible demand level 3
$M$	Large scalar value
$\Gamma_r$	Uncertainty budget for renewable unit

### Parameters

$dem_{n,t}$	Electricity demand at node and time step [MWh]
$ac_r$	Annualized investments costs for solar & wind generation units [EUR/MW]
$ac_b^{INV}$	Annualized investments costs for battery inverter of battery storage units [EUR/MW]
$ac_b^{STOR}$	Annualized investments costs for battery storage units [EUR/MWh]
$ac_h^{OCGT}$	Annualized investments costs for H <sub>2</sub> -fired open cycle gas turbine [EUR/MW]
$ac_h^{EL}$	Annualized investments costs for electrolyzer [EUR/MW]
$ac_h^{STOR}$	Annualized investments costs for H <sub>2</sub> storage [EUR/MWh]
$ac_l$	Annualized investment costs for transmission line [EUR/MW]
$vc_c$	Variable costs of conv. generation [EUR/MWh]
$sc_n^{LS1}$	Level 1 load shedding costs at node n [EUR/MW]
$sc_n^{LS2}$	Level 2 load shedding costs at node n [EUR/MW]
$sc_n^{LS3}$	Level 3 load shedding costs at node n [EUR/MW]
$\overline{cap}_c$	Existing conv. generation capacity [MW]
$\overline{cap}_{ror}$	Existing ror generation capacity [MW]
$\overline{cap}_{rsv}$	Existing rsv generation capacity [MW]
$\overline{cap}_{psp}$	Existing psp generation capacity [MW]

$\overline{cap}_l$	Existing transmission line capacity [MW]
$\overline{cf}_{r,t}$	Expected solar & wind capacity factors
$\overline{cf}_{r,t}^M$	Solar, wind capacity factors maximum deviation
$\overline{cf}_{r,t}^M$	Solar, wind capacity factors realization
$csf_{psp}$	Capacity scaling factor for pumping storage plants
$af_{rsv,t}$	Hydro reservoir availability factor
$\sigma_{psp}$	Efficiency of pumping storage plant
$\sigma_b$	Efficiency of battery inverter
$\sigma_h^{EL}$	Efficiency of electrolyzer
$\sigma_h^{OCGT}$	Efficiency of H <sub>2</sub> -fired open cycle gas turbine
$\overline{sub}_r^{REN}$	Solar, wind capacity in subproblem [MW]
$\overline{sub}_b^{INV}$	Capacity of battery inverter in subproblem [MW]
$\overline{sub}_b^{STOR}$	Battery storage capacity in subproblem [MWh]
$\overline{sub}_h^{OCGT}$	Capacity of H <sub>2</sub> -fired OCGT in subproblem [MW]
$\overline{sub}_h^{EL}$	Capacity of electrolyzer in subproblem [MW]
$\overline{sub}_h^{STOR}$	Hydrogen storage capacity in subproblem [MWh]
$\overline{sub}_l^{Line}$	Transmission line capacity in subproblem [MW]

### Positive Variables

$CAP_r$	Capacity of solar, wind generation unit [MW]
$CAP_b^{INV}$	Capacity of battery inverter unit [MW]
$CAP_b^{STOR}$	Storage capacity of battery unit [MWh]
$CAP_h^{OCGT}$	Capacity of H <sub>2</sub> -fired OCGT unit [MW]
$CAP_h^{EL}$	Capacity of electrolyzer unit [MW]
$CAP_h^{STOR}$	Storage capacity of hydrogen storage unit [MWh]
$CAP_l$	Transmission line capacity [MW]
$GEN_{c,t}$	Generation of conv. unit [MWh]
$GEN_{r,t}$	Generation of solar & wind unit [MWh]
$GEN_{ror,t}$	Generation of ror. unit [MWh]
$GEN_{rsv,t}$	Generation of rsv. unit [MWh]
$GEN_{psp,t}$	Generation of psp unit [MWh]
$CH_{psp,t}$	Charging of psp. unit [MWh]
$CH_{h,t}$	Charging of hydrogen storage [MWh]
$CH_{b,t}$	Charging of battery unit [MWh]
$LVL_{psp,t}$	Storage filling level of psp. unit [MWh]
$LVL_{b,t}$	Storage filling level of battery storage [MWh]
$LVL_{h,t}$	Storage filling level of hydrogen storage [MWh]
$LS_{n,t}^{L1}$	Load shedding level 1 [MWh]
$LS_{n,t}^{L2}$	Load shedding level 2 [MWh]
$LS_{n,t}^{L3}$	Load shedding level 3 [MWh]
$\overline{Cf}_{r,t}$	Uncertain renewable capacity factor

### Free Variables

$PF_{l,t}$	Line power flow [MWh]
$\theta_{s/r(l)}$	Voltage angle receiving/ sending line

### Binary Variables

$Z_{r,t}$	Variable representing the deviation from reference solar, wind capacity factor
-----------	--

### Auxiliary Variables

$\phi_{r,t}^{aux}$	Variable used for linearization
--------------------	---------------------------------

### Dual Variables

(·)	Dual variables are provided after the corresponding equalities or inequalities separated by a colon
-----	---

## Abstract

This study develops a capacity expansion model for a fully decarbonized European electricity system using an Adaptive Robust Optimization (ARO) framework. The model endogenously identifies the worst regional *Dunkelflaute* events, prolonged periods of low wind and solar availability, and incorporates multiple extreme weather realizations within a single optimization run. Results show that system costs rise nonlinearly with the geographic extent of these events: a single worst-case regional disruption increases costs by 9%, but broader disruptions across multiple regions lead to much sharper increases, up to 51%. As *Dunkelflaute* conditions extend across most of Europe, additional cost impacts level off, with a maximum increase of 71%. The optimal technology mix evolves with the severity of weather stress: while renewables, batteries, and interregional transmission are sufficient to manage localized events, large-scale disruptions require long-term hydrogen storage and load shedding to maintain system resilience. Central European regions, especially Germany and France, emerge as systemic bottlenecks, while peripheral regions bear the cost of compensatory overbuilding. These findings underscore the need for a coordinated European policy strategy that goes beyond national planning to support cross-border infrastructure investment, scale up flexible technologies such as long-duration storage, and promote a geographically balanced deployment of renewables to mitigate systemic risks associated with *Dunkelflaute* events.

# 1 INTRODUCTION

Limiting the increase in global average temperature to “well below” 2 °C leads to an energy transition towards nearly zero or even negative CO<sub>2</sub> emissions by mid-21<sup>st</sup> century (Rogelj et al., 2015; Davis et al., 2018). With sustained cost declines and increasing integration into the electricity supply mix, variable renewable energy technologies such as wind power and solar photovoltaic (PV) are expected to form the foundation of future low-carbon electricity system (Schlachtberger et al., 2017; Reichenberg et al., 2018; Brown et al., 2018; Mattsson et al., 2021). As low-carbon electricity systems based on variable renewable energy (VRE) are highly weather-dependent, weather-induced uncertainties, particularly the risk of prolonged periods of low renewable output, have become a central focus of both political discussions and academic research. Even in the English language, the German term “Dunkelflaute” has become popular to describe periods when the availability of wind and solar power is low, particularly the non-windy and non-sunny periods that manifest for an unusually long period e.g. days (Li et al., 2020, 2021a, 2021b; Mayer et al., 2023).

In Europe, weather-related uncertainties are addressed differently across regions due to the variability of regional weather regimes, as well as heterogeneous system characteristics and national policies. These differences reflect the diverse approaches that countries are taking to achieve carbon neutrality in the European Union (EU) by 2050.

The EU has made efforts to coordinate energy planning at a continental scale, including the development of joint scenarios by the European Network of Transmission System Operators for Electricity (ENTSO-E) through its Ten-Year Network Development Plan (TYNDP). However, managing weather-related uncertainties at this level remains challenging.<sup>1</sup>

A key difficulty lies in incorporating regional weather events such as *Dunkelflauten*. These events vary across Europe in frequency, intensity, and timing, often affecting countries unevenly. Yet their impacts can ripple across borders, disrupt electricity flows and threatening system stability well beyond the regions directly affected.

From a planning perspective, it is crucial that future energy systems are designed to withstand fluctuations in renewable resource availability without requiring costly short-term adjustments. This quality is often referred to as *robustness*. However, the concept of robustness is not consistently defined and is not linked to any specific methodology, making its application in energy system planning both essential and complex.

The development of mathematical optimization programs for energy system planning introduces various methodological approaches to address this challenge. Historically, most approaches exploring optimal energy systems were deterministic, based on expected or “typical” weather years. To ensure a certain level of robustness, such an optimization can be also based on a typical “worst-case” weather year. Alternatively, sampling over several historical weather years offers heuristic approaches to achieve robustness, such as averaging over the samples or imposing upper and lower bounds on generation capacities (Caglayan et al., 2021). However, a drawback is that these strategies are limited to analyzing uncertainty in a post processing step based on exogenous parameter changes, missing key tradeoffs within the decision making such as feedback loops.

Due to improvements in hardware and software, systematic approaches such as stochastic programming or robust optimization (RO) offer a possibility to account endogenously for uncertainties in the modelling. This has the advantage that the structure of uncertainty is directly incorporated in the program enabling it to replicate real world decision processes such as resource decisions. A broad range of possible applications of stochastic programming is presented in the literature, and is found to be a suitable method to address uncertainties in long-term energy system planning (Zakaria et al., 2020; Seljom et al., 2021). However, its practical application is often constrained by scalability issues (Birge and Louveaux, 2011; Baringo and Rahimiyan, 2020), particularly when accounting for a large set of possible weather regimes. The growing number of scenarios necessary to represent the possible realization space adequately counteracts the computational tractability. This necessitates tradeoffs in scenario selection, where a representative subset must balance accuracy and computational tractability. A key limitation of this approach is that the solution for scenarios excluded from the subset is not guaranteed, which is especially an issue when preparing for worst case realizations.

In contrast to stochastic programming, Robust Optimization (RO) seeks to find the optimal solution that is optimal to the worst possible realization of uncertainties (i.e., worst possible scenario). While RO offers advantages in terms of computational tractability and reduced problem complexity, this comes at the expense of solution conservatism. In the context of weather uncertainty, this means that the system is designed to withstand a rare extreme event, which may never actually occur.

---

<sup>1</sup> The TYNDP mission of ENTSO-E bases robustness on typical weather year computations, and the engagement of the European Union Agency for the Cooperation of Energy Regulators (ACER) employs stochastic programming using a reduced set of scenarios to tradeoff between accuracy and computational tractability.

Furthermore, classical RO does not include recourse actions—adaptive responses after uncertainty is realized—limiting its ability to model operational flexibility. As a result, the solution may lead to over-investment and suboptimal performance under other weather conditions, raising concerns about economic efficiency.

We address these difficulties by applying adaptive robust optimization (ARO) as a systematic approach to incorporate weather uncertainty into energy system planning. A major benefit of the ARO methodology consists of sequential decision-making, enabling model decisions to be adapted as the situation evolves. In this context, ARO iteratively identifies worst-case realizations of uncertain inputs - such as low wind and solar availability - and optimizes the system accordingly. Compared to stochastic programming, ARO provides a computationally more tractable framework, avoiding the exponential growth in scenario trees. At the same time, it results in less conservative and more cost-effective solutions than classical RO because of the adaptability in response to uncertainty. Therefore, ARO is particularly well-suited for energy systems exposed to weather-driven uncertainty, as it enables long term planning to incorporate a wide range of uncertainty realizations.

Building on the Adaptive Robust Optimization (ARO) framework, we develop a capacity expansion model to design a decarbonized electricity system for Europe in 2050 that is robust against periods of low wind and solar availability. Specifically, we represent low wind and solar availability events with varying geographical coverage across Europe, treating them as worst-case uncertainty realizations determined endogenously within the optimization. This enables the model also to account for periods where the simultaneous wind and solar availability in specific regions is low. To avoid confusion between general descriptive language and model-specific terminology, we introduce the following distinction: the term extreme weather event is used generically to describe periods of significantly reduced renewable generation—whether due to low wind, low solar, or both. In contrast, a worst-case low renewable availability weather event refers to a specific uncertainty realization identified within our ARO framework, representing the most adverse combination of renewable availability for system planning. If both wind and solar availability are simultaneously and severely reduced, we refer to this as a worst-case Dunkelflaute event. While all worst-case events are extreme, not every extreme weather event is a worst-case realization. To the best of our knowledge, this is the first study to apply a robust capacity expansion model to a fully decarbonized European electricity system in 2050 that endogenously identifies such worst-case weather events and incorporates their effects into the planning process. Specifically, we aim to:

1. Develop a methodology for designing a robust European electricity system that accounts for worst-case regional Dunkelflaute events.
2. Identify the worst-case regional Dunkelflaute events in Europe and quantify the direction and approximate magnitude of the impact on system costs and design when incorporating such weather events into long-term energy planning.

Our work provides a literature review on energy systems planning methods related to weather events such as Dunkelflaute, and the respective methodological modelling approaches in section 2. In section 3 we provide a brief overview and explanation of the concept behind the ARO method. Our case study is presented in section 4, and the results are discussed in section 5. We finish the paper with conclusions and a summary of the key takeaways in section 6.

## 2 LITERATURE REVIEW

Long-term energy system planning, considering extreme weather events, has become increasingly popular over the last two decades. Extreme weather event analyses have focused on several aspects. A smaller part of the body of literature explores how extreme events such as floods and (ice) storms impair energy infrastructure. The majority of papers explore weather events which impact supply and demand. Examples are heatwaves and cold periods, hydro droughts, and low solar and wind availability periods. All these topics of interest have become relevant for electricity system planning. Especially, reduced output of intermittent RES is facing popular interest in the academic world, and beyond.<sup>2</sup> For the European energy system, the impact of reduced RES availability is of major interest since a 100% renewable European system in 2050 will heavily rely on wind and solar generation technologies. Therefore, several academic studies investigate such weather events and their impacts, as well as the requirements on the current and future electricity systems in order to guarantee a reliable energy supply.

These investigations can be distinguished as (1) meteorologically-based approaches, which describe historical extreme weather events (e.g. Ohlendorf and Schill, 2020; Li et al., 2020, 2021a, 2021b; Jurasz et al., 2021), (2) modeling-based investigations, focusing on including weather-related uncertainties into the system planning (e.g. Jabr, 2013; Roldán et al.,

---

<sup>2</sup> Some examples: Quartz: <https://qz.com/can-europe-survive-the-dreaded-dunkelflaute-1849886529>, Reuters: <https://www.reuters.com/markets/commodities/german-wind-reliant-power-firms-brace-annual-dunkelflaute-2024-02-21/>, a children’s book named “Dunkelflaute: A Story of Renewable Wind Power” by Stephanie O’Connor (2022), Madra Rua Publishing, Donegal, Ireland.

2018; Roldán et al., 2019; Roldán et al., 2020), and (3) approaches employing both, connecting meteorological weather data and empirical modeling applications (Raynaud et al., 2018; Hannah C. Bloomfield et al., 2020; H. C. Bloomfield et al., 2020; Otero et al., 2022a; Ruhnau and Qvist, 2022; Grochowicz et al., 2024a). Given that our study focusses on modelling extreme weather events within an energy system optimization framework, we place particular emphasis on reviewing the latter two categories, which align most closely with our aim and scope.

In 2013 Jabr designed a robust model to include the uncertainty from renewable generation and electricity load in the transmission network expansion planning process using a cardinality-constrained uncertainty set. The developed bi-level optimization problem was iteratively solved using Bender's decomposition approach (an iterative technique for mathematical programming). Testing and comparing the proposed model on various test grid systems showed that the method consistently generated reliable and cost-effective expansion plans. In a series of follow-up papers, Roldán et al., (2018, 2019, 2020) present robust model formulations, to tackle the incorporation of weather uncertainties into the transmission and generation expansion planning problem. A three-level adaptive robust optimization program was introduced to include uncertainty from wind turbines in a dynamic investment setting covering 25 years (Roldán et al., 2018). To address the disregarded correlation of uncertainty sources such as wind speed, Roldán et al. (2019) turn from using cardinal and polyhedral sets towards so-called ellipsoidal uncertainty sets. The newly developed two-stage adaptive robust optimization approach was developed further by Roldán et al. (2020) to consider the complete probability structure of uncertainty parameters, ensuring that the optimal solution found is valid. Baringo et al. (2020) developed an adaptive robust optimization model to address the expansion planning of a distribution system that incorporates solar powered electric vehicles and energy storage systems. The model considers both short-term variabilities, such as daily demand patterns, renewable variation, and long-term uncertainty, such as future peak demand and the penetration of electric vehicles. The ARO methodology proves to be an effective tool for distribution expansion planning by highlighting that incorporating long-term uncertainty significantly influences investment decisions.

As these studies are conducted on test grid systems to validate the efficiency of the optimization approaches, the transfer of the implications on a national energy system are limited. Also, the impact of extreme weather events, such as Dunkelflauten, remain unaddressed. In order to incorporate the weather-related uncertainty in real-world energy system planning, the body of literature offers a huge collection of papers using different solution approaches and case studies. An overview is provided by, for example, Yue et al. (2018) and Conejo and Wu (2022), in which the latter points towards robust optimization methodologies used for power system planning. As this study focuses on the potential impacts and challenges of worst-case weather events affecting wind and solar availability in a future decarbonized European electricity system, the following section provides a brief overview of relevant European case studies.

The interplay between meteorological and statistical analysis of weather data related to solar, wind, and electricity-demand time series is investigated, e.g. in studies from Raynaud et al. (2018), Wiel et al. (2019), H. C. Bloomfield et al. (2020) and Otero et al., (2022a).

Raynaud et al. (2018) researched variations of so called energy supply and production droughts across Europe and found that the individual drought which the countries under study experience ranged between one to seven days in duration. While wind droughts occur more often and are present for a short period of up to three days on average for most countries, solar drought follows more of a geographical and seasonal pattern, leading to Nordic counties being more exposed to longer lasting energy drought events. Wiel et al. (2019) examined the role of weather regimes in explaining daily variations in solar PV, wind output, and electricity demand. They show that a certain day-to-day variability can be explained by identified weather regimes, which can be detected and forecasted providing valuable information for the system operating. However, the authors also state that rare extreme events cannot be precisely predicted. H. C. Bloomfield et al. (2020) studied how solar and wind generation align with demand during system stress events. They concluded that the potential of renewables to reduce residual load is limited during extreme conditions, and interconnectivity offers only marginal relief during high-demand and low-availability periods. Otero et al. (2022a) focused on compound periods of low wind and solar generation coinciding with high demand. They showed that such events often affect multiple European countries simultaneously, underlining the systemic risk posed by these conditions.

While the studies above highlight country-specific patterns of low solar and wind availability, they rely on simplified modeling assumptions, often excluding storage, transmission, and broader generation portfolios. As such, they offer limited insights into how future energy systems might adapt to these conditions. The following section reviews studies that incorporate weather uncertainty into energy system optimization models, with a focus on Europe.

Perera et al. (2020) developed a stochastic-robust optimization method to investigate the impact of extreme events using 13 climate change scenarios on 30 cities in Sweden. They state that future climatic fluctuations and extreme weather events must be incorporated into the energy system planning using suitable methods to incorporate this uncertainty endogenously. Failing

to do so could hinder the integration of renewable energy into future systems and compromise the reliability of energy supply. However, the focus on Swedish cities limits the broader applicability of the findings to the European system.

By employing a deterministic multi-year energy system optimization model, Ruhnau and Qvist (2022) investigated low renewable availability events within the context of a German market that would be fully powered by renewable energy systems in 2050. They analyze a period of 35 historical years, highlighting that periods of low renewable availability can continue for up to two weeks duration. However, they also point out that the biggest energy shortfall can cover a substantially longer period of up to nine weeks. The authors argue that focusing on short-duration extreme events or single years may result in underestimating both the storage requirements and costs of a system supplied solely by renewable sources.

Plaga and Bertsch (2022) apply a robust optimization approach to European electricity system planning under climate uncertainty, using six climate scenarios from the Euro-Cordex database. The results show that the system cost varies between the cheapest and most expensive scenarios by around 24 percent. Furthermore, the results show that in the robust optimization more generation and battery storage capacity is built, increasing the system cost by another 3 percent compared to the most expensive deterministic scenario. While their analysis focuses on system costs, generation capacity, and loss of load, it provides limited insights into the specific characteristics of weather events.

Grochowicz et al. (2023a) employed a near-optimal space method to generate a robust European power system. Their geometric concept involves mapping the individual near-optimal feasible spaces from single weather-year optimizations, and selecting a single solution at the geometric center, providing a certain tolerance towards infeasibility across all considered periods. By dispatching over the attained geometric-centered system layout, they found that more onshore wind and solar power is installed, leading to a 50% CO<sub>2</sub> emissions reduction compared to a cost optimal solution. By restricting their feasibility space on investment costs, the nodal generation capacities may vary within the optimal solution and the impact of region-specific contributions remains unaddressed.

Another article by Grochowicz et al. (2024), investigates weather induced system stress on the European electricity system using nodal shadow prices as an indicator. They found that the most extreme periods happen between November and February with an average duration of 7 days. While the single year optimizations entail important information on the system adoptions possibilities, a robust system layout is not provided.

Gøtske et al. (2024) assess the impact of 62 historical weather years on a future sector-coupled, decarbonized European energy system using the PyPSA-Eur model. They conduct individual capacity optimizations for each weather year and then test the robustness of the resulting layouts by performing dispatch optimizations across all other years. Their findings highlight that low wind availability during winter poses the greatest challenge to system stability. However, since the study relies on a deterministic modeling approach, the robust system layout is effectively tailored to a single worst-case weather year. This limits the analysis's ability to evaluate trade-offs between capacity expansion and the broader spectrum of possible weather events not captured by that specific year.

In summary, the existing literature largely falls into two categories: studies applying robust modeling techniques to stylized test systems with weather-related risks, and studies integrating meteorological weather data into simplified real-world electricity systems. However, only a few contributions systematically incorporate the risk of extreme low solar and wind availability events across Europe by either deterministically sampling over a large weather data set or using a robust optimization framework.

We identify a research gap centered around the question: *What if a planning model could endogenously determine when and where worst-case low renewable availability events occur—and proactively prepare for them?*

To address this, our study presents a methodological framework for a robust energy system model that endogenously integrates realizations of regional low solar and/or wind generation periods within a future European electricity system. This approach enables us to analyze how the system adapts to extreme events, providing insights into the inherent trade-offs in long-term planning by increasing incrementally stress on the system.

### 3 METHODOLOGY

In this study we formulate a long-term generation and transmission expansion planning problem from a central planner's perspective. The energy system model optimizes investment decisions under uncertainty using the ARO method. First, we provide an overview of a general expansion problem formulation, and how it is integrated into the ARO framework. Second, we introduce the uncertainty formulation. Third, we explain the solution strategy for this optimization problem.

### 3.1 Expansion Planning and Adaptive Robust Optimization

In general, expansion problems address the need to plan how future demand can be met with scarce resources, and they aim to either maximize or minimize the objective criteria under certain technical constraints. In the context of the electrical energy system, the aim is to identify how future energy needs can be met, investing in generation assets and transmission lines to meet the demand (Conejo et al., 2016). A typical optimization problem from a central planner's perspective could look like the following:

$$\begin{aligned}
 & \text{(i) } \text{Min}_x \text{ } IC^T x \\
 & \text{s.t.} \\
 & \quad h(x) = 0 \\
 & \quad g(x) \leq 0
 \end{aligned}$$

The objective function (i) minimizes the total system costs, which are the product of a vector  $x$ , representing an investment decision and the investment cost vector  $IC^T$ . In addition, certain equality conditions  $h(x)$ , such as supply, need to meet demand, and inequality conditions  $g(x)$ , such as that the generation is limited to the nominal capacity, must be satisfied. This problem formulation enables uncertainty to be incorporated exogenously by changing uncertain parameters and formulating deterministic scenarios, analyzing the results ex-post. On the contrary, adaptive robust optimization incorporates uncertainty in an endogenous manner, thus adding two extra layers of complexity. The aim of the robust optimization approach is to find model solutions that are immune to the worst-case uncertain perturbations within their predefined confidence bounds. In what follows, we refer to this solution as the robust solution. In ARO problems, decisions are modeled beyond this with recourse, making the solution robust to all combinations of uncertainty defined by a so-called uncertainty budget. This strategy results in a three-level optimization problem which can be formulated as follows:

$$\begin{array}{lll}
 \text{(i) } \text{Min}_x \text{ } IC^T x & \text{(ii) } \text{Max}_u & \text{(iii) } \text{Min}_y \text{ } [OC(x, u)]^T y \\
 \text{s.t.} & \text{s.t.} & \text{s.t.} \\
 h(x) = 0 & u \in U & y \in \Omega(x, u) = \{ \\
 g(x) \leq 0 & & A(x, u)y = b(x, u): \lambda \\
 & & D(x, u)y \geq e(x, u): \mu \}
 \end{array}$$

Here, the deterministic problem (i) represents solely the first stage of the optimization process, thus minimizing the system costs prior to the uncertainty realization. Based on this solution, the second level (ii) aims to maximize the total system costs by finding the worst-case realizations, represented by the variable vector  $u$ . The second-stage decision variable is bounded by the confidence bounds of the possible uncertainty realization space  $U$ , which could be, for example, the “on” or “off” status of a power plant. The third level encompasses the corrective actions, aiming to minimize total system operation costs  $OC$  based on the prior results  $(x, u)$  of level (i) and (ii). These actions are represented by variable vector  $y$ , and bounded by the feasibility space  $\Omega(x, u)$  which is the constraining level (iii) based on (i) and (ii). Consequently  $A, b, D, e$  are matrices with constant parameters and  $\lambda$  and  $\mu$  represent the dual variables associated with equality and inequality constraints. In the context of the electricity energy system model, these actions would correspond to, for example, technical constraints of power plants in the dispatch process. This problem structure enables the model to address uncertainty endogenously, following the typical chronological order of decision making, uncertainty realization, and reaction in an infrastructure planning process (Ruiz and Conejo, 2015).

### 3.2 Modeling Uncertainty

To model uncertainty in the second-level problem (ii), we employ polyhedral uncertainty sets, introduced by Bertsimas and Sim (2004). More specifically, we use a cardinality-constrained polyhedral uncertainty set, which allows us to adjust the level of robustness, by controlling the number of uncertain coefficient perturbations within a constraint. This number is represented by the so-called uncertainty budget  $\Gamma$ , which guarantees that the solution of the model is protected against all cases up to  $\Gamma$  coefficients that can deviate from their nominal value.

In our second-level problem, the uncertainty is represented by the decision variable  $u$ , which can take values within specified confidence bounds:

$$u \in \{\tilde{u} - \hat{u}, \tilde{u} + \hat{u}\}$$

Here,  $\tilde{u}$  and  $\hat{u}$  are specifying the expected nominal value and the maximum deviation value. We follow the definition of the cardinality-constrained uncertainty set  $\Omega$  as described by Mínguez and García-Bertrand (2016) and Baringo et al. (2020):

$$\Omega = \left\{ \begin{array}{l} u = \tilde{u} + \text{diag}(z^+) \hat{u} - \text{diag}(z^-) \hat{u}, \\ z^+, z^- \in \{0,1\}^n, \\ \sum_{k=1}^n (z^+ + z^-) \leq \Gamma \\ z^+ + z^- \leq 1 \end{array} \right\}$$

Here, the value of  $u$  depends on the binary variables  $z^+, z^-$ , which decide whether  $u$  deviates from its nominal value towards the upper or lower bound, or not. To control the level of robustness,  $\Gamma$  is restricting the number of deviations. A value of  $\Gamma = 0$  leads to the realization of the expected value  $u = \tilde{u}$ , while any other discrete positive value of  $\Gamma$  implies that  $u$  can deviate from the expected value, which represents an uncertainty realization. Hence,  $u$  cannot take values of the upper and lower bounds at the same time, and the simultaneous realization of  $z^+$  and  $z^-$  is excluded.

### 3.3 Solution Strategy

The solution strategy on solving the three-level optimization problem is based on the literature stream established by Bertsimas et al. (2013), Mínguez and García-Bertrand (2016), Zhang and Conejo (2018), and Baringo et al. (2020). The first step is to couple the second level (ii) and the third level (iii) of the optimization problem, making it a single optimization problem. The second step is to linearize the new second level, and employ a column and constraint algorithm to solve the remaining two-level optimization problem in an efficient manner. In the following, we provide a short explanation of these processes. However, the interested reader is referred to the work of Baringo and Rahimiyan (2020) and Riepin et al. (2021) which provide a more detailed explanation.

In order to couple the third level (iii) with the second level (ii) optimization problem, we assume that problem (iii) is linear, and thus convex. On this basis we know that the dual problem solution equals the primary problem (strong duality). The reformulation of the third-level problem into its dual pendant (iii') is shown in the following:

$$\begin{array}{ll} \text{(iii) } \text{Min}_y [OC(x, u)]^T y & \text{(iii') } \text{Max}_{\lambda, \mu} B(x, u) \cdot \lambda + E(x, u) \cdot \mu \\ \text{s.t.} & \text{s.t.} \\ y \in \Omega(x, u) = \{ & A(x, u) \cdot \lambda + D(x, u) \cdot \mu = OC(x, u) \\ A(x, u)y = b(x, u): \lambda & \lambda: \text{free}, \mu \geq 0 \\ D(x, u)y \geq e(x, u): \mu \} & \end{array}$$

As a next step, the dual reformulated problem (iii') is merged with level (ii), resulting in a single optimization problem (II). The new two-level min (I) – max (II) optimization problem is as stated below:

$$\begin{array}{ll} \text{(I) } \text{Min}_x IC^T x & \text{(II) } \text{Max}_{u, \lambda, \mu} [b(x, u)]^T \lambda + [D(x, u)]^T \mu \\ \text{s.t.} & \text{s.t.} \\ h(x) = 0 & A(x, u)\lambda + D(x, u)\mu = OC(x, u) \\ g(x) \leq 0 & u \in U, \lambda: \text{free}, \mu \geq 0 \end{array}$$

As there is a bilinear term  $[b(x, u)]^T \lambda$  in the objective function of the subproblem (II), it makes this formulation a Mixed-Integer Nonlinear Programming (MINLP) and thus is hard to solve. Therefore, big-M constraints are employed to reformulate this term, adding an auxiliary variable, making the problem a Mixed-Integer Linear Programming (MILP), which is easier to solve. This process is explained in more detail by Baringo and Rahimiyan, (2020). At this point, the Master Problem (I) and the Subproblem (II) are established, which can be iteratively solved using the column and constraint generation algorithm. During this process, the Master Problem transfers expansion information in set  $\Phi^{M \rightarrow S}$  to the Subproblem, which sends back information about worst case realizations and corrective actions in set  $\Phi^{S \rightarrow M}$  to the Master Problem, visualized in Figure 1. This process continues until the objective values of both problems converge to a previously defined value. The interested reader is referred to the book by Conejo et al. (2016), which details an extensive explanation of the column and constraint generation algorithm.

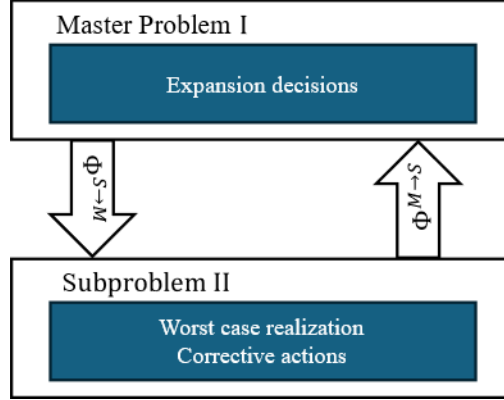


Figure 1. Iterative ARO solution approach, based on the work of Baringo et al. (2020).

## 4 APPLICATION – CASE STUDY

For our study we develop a generation and transmission expansion planning model for a 100% renewable European electricity system with the planning horizon of 2050.

We represent the European high-voltage electricity system using a mixed-integer linear programming (MILP) model based on the linearized (DC) optimal power flow method with the objective function to minimize the investment and generation costs.

By applying the ARO method, we investigate the effects of endogenously modeled “Dunkelflauten” on system metrics such as costs and the technology mix. In this section, first we introduce the deterministic model setup. Second, we describe the parameterization of weather-related solar and wind uncertainty. Third, we present the ARO model formulation. Finally, we define the investigated scenarios. To support transparency and reproducibility, all data, code, and results are publicly available on GitHub<sup>3</sup>, allowing readers to verify, adapt, or extend our work.

### 4.1 Expansion Model and Parameterization

The transmission and generation expansion planning model is formulated as a deterministic linear problem where the optimization variables are denoted in the set  $\Phi^D = \{ CAP_{pv}; CAP_{wind}; CAP_b^{INV}; CAP_b^{STOR}; CAP_h^{OCGT}; CAP_h^{EL}; CAP_h^{STOR}; CAP_l; GEN_{c,t}; GEN_{r,t}; GEN_{ror,t}; GEN_{rsv,t}; GEN_{psp,t}; CH_{psp,t}; CH_{h,t}; CH_{b,t}; LVL_{psp,t}; LVL_{b,t}; LVL_{h,t}; PF_{l,t}; S_{n,t}^{LS1}; S_{n,t}^{LS2}; S_{n,t}^{LS3}; \theta_{s/r(t)} \}$ :

$$\begin{aligned}
 \text{Min}_{\Phi^D} : & \sum_{pv} CAP_{pv} \cdot ac_{pv} + \sum_{wind} CAP_{wind} \cdot ac_{wind} \\
 & + \sum_b CAP_b^{INV} \cdot ac_b^{INV} + \sum_b CAP_b^{STOR} \cdot ac_b^{STOR} + \sum_h CAP_h^{OCGT} \cdot ac_h^{OCGT} + \sum_h CAP_h^{EL} \cdot ac_h^{EL} \\
 & + \sum_h CAP_h^{STOR} \cdot ac_h^{STOR} + \sum_l CAP_l \cdot ac_l + \sum_{c,t} GEN_{c,t} \cdot vc_c + \sum_{n,t} LS_{n,t}^{L1} \cdot sc_n^{LS1} \\
 & + \sum_{n,t} LS_{n,t}^{L2} \cdot sc_n^{LS2} + \sum_{n,t} LS_{n,t}^{L3} \cdot sc_n^{LS3}
 \end{aligned} \tag{1}$$

subject to

<sup>3</sup> [https://github.com/bernemax/ARO\\_Dunkelflaute\\_Europe](https://github.com/bernemax/ARO_Dunkelflaute_Europe)

$$dem_{n,t} - LS_{n,t}^{L1} - LS_{n,t}^{L2} - LS_{n,t}^{L3} \quad (2)$$

$$= \sum_{r \in \Phi_n^{pv}} GEN_{pv,t} + \sum_{r \in \Phi_n^{wind}} GEN_{wind,t} + \sum_{c \in \Phi_n^c} GEN_{c,t} + \sum_{ror \in \Phi_n^{ROR}} GEN_{ror,t} + \sum_{rsv \in \Phi_n^{RSV}} GEN_{rsv,t} \\ + \sum_{psp \in \Phi_n^{PSP}} (GEN_{psp,t} - CH_{psp,t}) + \sum_{h \in \Phi_n^H} (GEN_{h,t} - CH_{h,t}) + \sum_{b \in \Phi_n^B} (GEN_{b,t} - CH_{b,t}) \\ + \sum_{l \in r(l)} PF_{l,t} - \sum_{l \in s(l)} PF_{l,t} : \lambda_{n,t}, \forall n, t$$

$$GEN_{pv,t} \leq CAP_{pv} \cdot \widetilde{cf}_{pv,t} : \mu_{pv,t}^R, \forall pv(r), t \quad (3)$$

$$GEN_{wind,t} \leq CAP_{wind} \cdot \widetilde{cf}_{wind,t} : \mu_{wind,t}^R, \forall wind(r), t \quad (4)$$

$$GEN_{c,t} \leq \overline{cap}_c : \mu_{c,t}^{Conv}, \forall c, t \quad (5)$$

$$GEN_{ror,t} \leq \overline{cap}_{ror} : \mu_{ror,t}^{ROR}, \forall ror, t \quad (6)$$

$$GEN_{rsv,t} \leq \overline{cap}_{rsv} \cdot af_{rsv,t} : \mu_{rsv,t}^{RSV}, \forall rsv, t \quad (7)$$

$$GEN_{psp,t} \leq \overline{cap}_{psp} : \mu_{psp,t}^{DIS}, \forall psp, t \quad (8)$$

$$CH_{psp,t} \leq \overline{cap}_{psp} : \mu_{psp,t}^{CH}, \forall psp, t \quad (9)$$

$$LVL_{psp,t} \leq \overline{cap}_{psp} \cdot csf_{psp} : \mu_{psp,t}^{CAP}, \forall psp, t \quad (10)$$

$$LVL_{psp,t=1} = \frac{(cap_{psp} \cdot csf_{psp})}{2} + (CH_{psp,t=1} \cdot \sigma_{psp}) - GEN_{psp,t=1} : \phi_{psp,t=1}^{LVL}, \forall psp \quad (11)$$

$$LVL_{psp,t} = LVL_{psp,t-1} + (CH_{psp,t} \cdot \sigma_{psp}) - GEN_{psp,t} : \phi_{psp,t}^{LVL}, \forall psp, \forall t > 1, \quad (12)$$

$$GEN_{b,t} \leq CAP_b^{INV} : \mu_{b,t}^{DB}, \forall b, t \quad (13)$$

$$CH_{b,t} \leq CAP_b^{INV} : \mu_{b,t}^{CB}, \forall b, t \quad (14)$$

$$LVL_{b,t} \leq CAP_b^{STOR} : \mu_{b,t}^{CAP}, \forall b, t \quad (15)$$

$$LVL_{b,t=1} = (CH_{b,t=1} \cdot \sigma_b) - GEN_{b,t=1} : \phi_{b,t=1}^{LVLB}, \forall b \quad (16)$$

$$LVL_{b,t} = LVL_{b,t-1} + (CH_{b,t} \cdot \sigma_b) - GEN_{b,t} : \phi_{b,t}^{LVLB}, \forall b, \forall t > 1, \quad (17)$$

$$GEN_{h,t} \leq CAP_h^{OCGT} : \mu_{h,t}^{OCGT}, \forall h, t \quad (18)$$

$$CH_{h,t} \leq CAP_h^{EL} : \mu_{h,t}^{EL}, \forall h, t \quad (19)$$

$$LVL_{h,t} \leq CAP_h^{STOR} : \mu_{h,t}^{CAPH}, \forall h, t \quad (20)$$

$$LVL_{h,t=1} = (CH_{h,t=1} \cdot \sigma_h^{EL}) - \frac{GEN_{h,t=1}}{\sigma_h^{OCGT}} : \phi_{h,t=1}^{LVLH}, \forall h \quad (21)$$

$$LVL_{h,t} = LVL_{h,t-1} + (CH_{h,t} \cdot \sigma_h^{EL}) - \frac{GEN_{h,t}}{\sigma_h^{OCGT}} : \phi_{h,t}^{LVLH}, \forall h, \forall t > 1, \quad (22)$$

$$PF_{l,t} = sus_l \cdot (\theta_{s(l)} - \theta_{r(l)}) : \phi_{l,t}^l, \forall l, t \quad (23)$$

$$-(\overline{cap}_l + CAP_l) \leq PF_{l,t} \leq \overline{cap}_l + CAP_l : \underline{\mu}_{l,t}^l, \overline{\mu}_{l,t}^l, \forall l, t \quad (24)$$

$$-\pi \leq \theta_{n,t} \leq \pi : \underline{\mu}_{n,t}^N, \overline{\mu}_{n,t}^N, \forall n, t \quad (25)$$

$$\theta_{n,t} = 0 : \epsilon^{ref}, \quad n \in ref(n) \quad (26)$$

$$LS_{n,t}^{L1} \leq dem_{n,t} \cdot f^{L1} : \mu_{n,t}^{LS1}, \forall n, t \quad (27)$$

$$LS_{n,t}^{L2} \leq dem_{n,t} \cdot f^{L2} : \mu_{n,t}^{LS2}, \forall n, t \quad (28)$$

$$LS_{n,t}^{L3} \leq dem_{n,t} \cdot f^{L3} : \mu_{n,t}^{LS3}, \forall n, t \quad (29)$$

The objective function in Eq. (1) minimizes the sum of the annualized renewable capacity and transmission investment costs, the annualized costs of the battery storage systems, which includes inverter and storage cost components, the annualized costs of the hydrogen storage systems, which include the electrolyzer, the H<sub>2</sub> storage tank and the H<sub>2</sub> fired open cycle gas turbines (OCGTs) power plant, as well as the variable generation costs and the load shedding costs. The minimization problem is subject to several constraints such as the energy balance in Eq. (2), the technical generation constraints of renewable generation units, considering the expected capacity factors for solar PV and wind ( $\widetilde{c}_{pv,t}, \widetilde{c}_{wind,t}$ ) in Eqs. (3-4), the conventional generation in Eq. (5), and hydropower generation in Eqs. (6-7), the storage constraints for pumping storage plants in Eqs. (8-12), battery storages in Eqs. (13-17) and hydrogen storage in Eqs. (18-22), the power flow constraints in Eqs. (23-26), and the load shedding constraints in Eqs. (27-29). Note that these three load shedding constraints establish a stepwise load shedding curve, where the factors  $f^{L1}, f^{L2}, f^{L3}$  (with  $f^{L1} < f^{L2} < f^{L3}$ ) represent specific percentages of demand at a given node and time. The load shedding variables  $LS_{n,t}^{L1}, LS_{n,t}^{L2}, LS_{n,t}^{L3}$  are multiplied with different cost levels in the objective function. This implementation creates a stepwise load shedding cost function, enabling the model to utilize varying degrees of load flexibility at different cost levels.

We use the Python for Power System Analysis of the Euro power system model (PyPSA-Eur) to cluster the underlying GRID-Kit transmission system data to generate the underlying energy system with 50 nodes and 97 lines across 24 countries. The model differentiates expandable and non-expandable generation technologies. Expandable generation technologies allow endogenous investment in new capacity comprising solar PV, onshore wind, offshore wind (where coastal connections exist), hydrogen storage, electrolyzers, hydrogen-fired open cycle gas turbines (OCGT), battery storage, and inverters. Also, the transmission line capacity can be expanded. However, expansion is limited to an additional 100 % of 2020 levels (i.e. ENTSOE's TYNDP 2024 assumes up to 75 % by 2040). Non-endogenous capacities comprise hydro and nuclear power. We fix hydro power, which includes run-of-river (ROR), reservoir and pumping storage power plants, at their current levels since we assume that expansion potential is negligible. For nuclear power capacity in 2050, we consider existing power plants that will still be in operation in 2050, given a lifetime of 60 years, as well as newly planned nuclear power projects based on data from the World Nuclear Association. Appendix A provides a visualization of the modeled system, as well as data on cost and technology.

The electricity demand for each node in 2050 was estimated using the open-source GlobalEnergyGIS package based on Mattsson et al. (2021). First, we projected annual electricity consumption for each region in 2050 based on 2016 demand data taken from the International Energy Agency, and regional growth in the Shared Socioeconomic Pathway 2 scenario from Riahi et al. (2017). Then, we estimated the hourly demand profile using a machine learning model that applies historical demand data from 44 countries to a gradient boosting regression approach based on Friedman (2001). This model incorporates calendar effects (e.g. hour of day, weekday/weekend), temperature (e.g. hourly temperature in key population areas), and economic indicators (e.g. local gross domestic product per capita). Finally, the hourly demand series is scaled to match the projected annual demand for each region in 2050.

To incorporate weather data, we analyzed 40 historical weather years based on data from the Renewable.ninja website (data are based on the works of Pfenninger and Staffell (2016), and Staffell and Pfenninger (2016)). For each node in the system, we include individual historical average capacity factor time series for solar PV, and onshore and offshore wind technologies. To enhance the model's tractability, we apply a time series reduction method (moving average) on the demand and renewable capacity factor time series. Consequently, our model includes an entire year with 4-hour timesteps.

## 4.2 Uncertainty Incorporation

To assess which combination of generation, storage, and transmission technologies ensures the robustness of the future EU electricity system against worst-case realizations of extreme low availability events, we stress-tested the investment model using synthetic extreme weather scenarios. Our methodology for modeling these worst-case weather events consisted of two main steps. In the first step, we defined the geographical scope, introducing weather regions within Europe. In these regions, solar and wind availability can be modeled either as typical availability conditions or as extreme low availability scenarios. In the second step, we defined the uncertainty realization space by specifying the number of affected regions, using a cardinality-constrained uncertainty set. In the following, we outline our methodology, first addressing the geographic scope of the extreme events, and then describing the cardinality-constrained uncertainty set.

### 4.2.1 Geographical Scope

In order to incorporate the effects of weather events with low solar and wind availability, our approach relied on splitting the modeled European system into six weather regions. Therefore, we assigned 24 European countries to these regions in accordance with the study by Otero et al., (2022), as shown in Figure 2. Those authors analyzed the correlation between the

monthly frequencies of energy compound events (periods with low wind and solar irradiance) among different European countries, considering the spatial relationship between critical energy events across Europe.

Within these regions we assume that the weather conditions, which translate back to the nodal renewable capacity factors, are the same: normal availability or low solar availability or low wind availability, or both low solar availability and low wind availability. In section 4.2.2, we outline how we modeled the realization of extreme weather conditions.

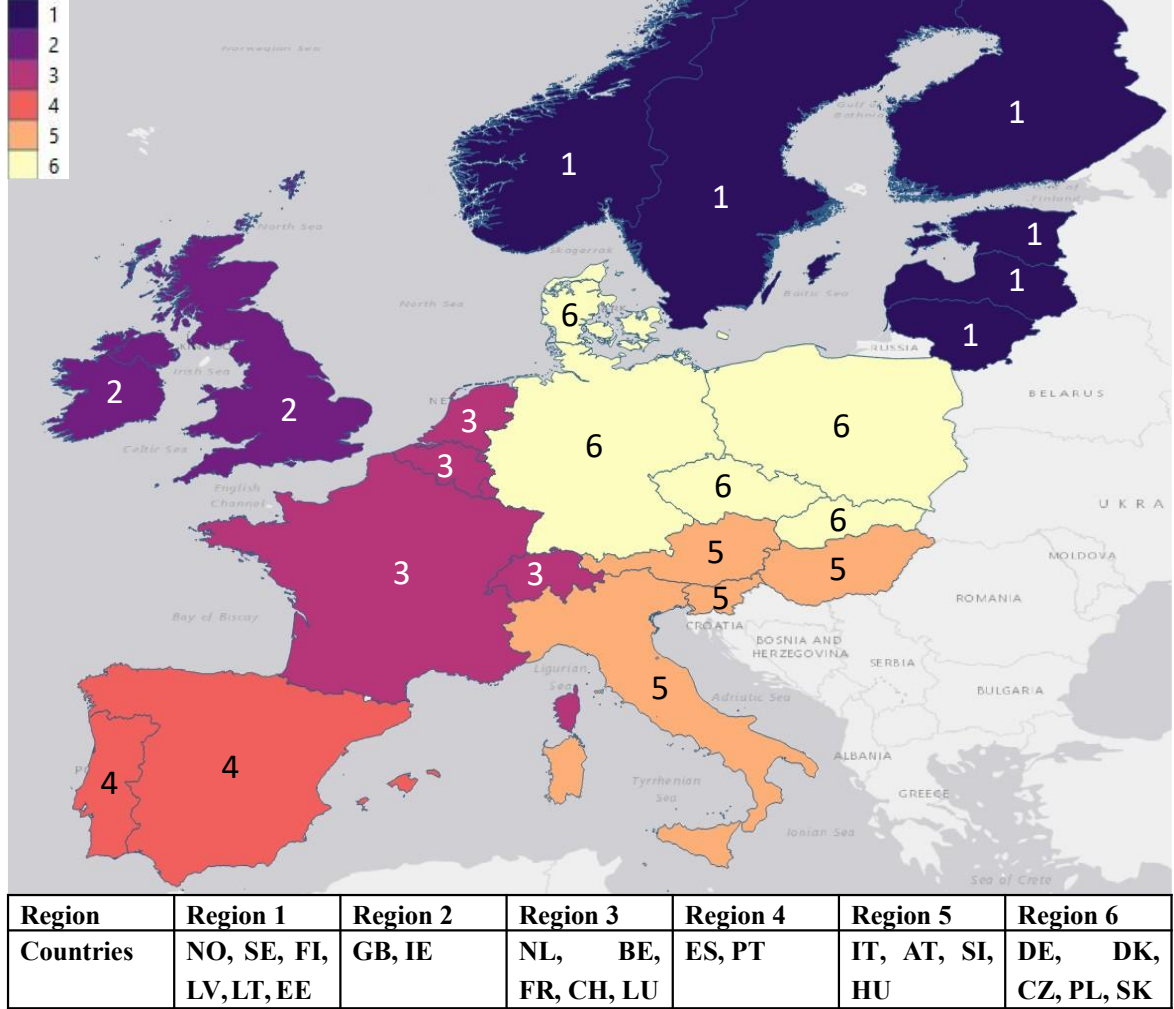


Figure 2. Map of weather regions – own illustration.

#### 4.2.2 Renewable Uncertainty - Capacity Factors Lower Bounds

Our approach to modeling uncertainty as the realization of low solar PV and wind availability involves defining cardinality-constrained uncertainty sets for these renewable generation technologies. The cardinality-constrained uncertainty set  $\Phi^U$  controls the number of uncertain parameters that can deviate from their nominal values. This is controlled by binary variables  $Z$  in combination with the uncertainty budget  $\Gamma$ , and can be described formally as follows:

$$\Phi^U = \left\{ \begin{array}{l} \overline{c}f_{r,g,t} = \widetilde{c}f_{r,g,t} - \sum_{p \in P(t)} Z_{r,g,p} \cdot \widehat{c}f_{r,g,t} \quad \forall r, \forall g, \forall t, \forall p \\ Z_{r,g,p} \in \{0,1\} \quad \forall r, \forall g, \forall p \\ \sum_{g \in G} Z_{r,g,p} \leq \Gamma_{r,p} \quad \forall r, \forall p \end{array} \right. \quad \begin{array}{l} (30) \\ (31) \\ (32) \end{array}$$

Equation (30) describes the uncertain renewable capacity factor  $\overline{c}f_{r,n,g,t}$  for a specific renewable technology  $r$  (solar PV or wind), located in weather region  $g$  and time step  $t$  depending on the reference value  $\widetilde{c}f_{r,g,t}$  (expected historical average) and the deviation values  $\widehat{c}f_{r,g,t}$ . The realization of the deviation depends on the value of the binary variable  $Z_{r,g,p}$ , defined by eq. (31). Note here, that the binary variable is defined over a certain period  $p$ . The period  $p$  is defining a time horizon, spanning over several timesteps, such as a day, week, or month including several hours. In our case study, we define the duration of this

period as one week (7 days), which corresponds to a time span of a worst case Dunkelflaute event (Raynaud et al., 2018; Li et al., 2021b; Otero et al., 2022b). The realization of  $Z_{r,g,p}$  is controlled by the uncertainty budget  $\Gamma_{r,p}$  as defined in eq. (32). The budget controls the number of deviations in solar or wind availability from their reference values across the defined weather regions and time periods. Here  $\Gamma_{r,p} = 0$  implies that no uncertainty occurs for the specific generation technology, meaning that the renewable capacity factor time series remains at its expected reference values for all regions. For all discrete values  $\Gamma_{r,g} \geq 0$ , a low renewable availability period can occur in a specific weather region as the deviation value  $\widehat{cf}_{r,g,t}$  is subtracted from the reference value. To determine  $\widehat{cf}_{r,g,t}$ , we generated a synthetic extreme low-capacity factor time series which serves as a so-called lower bound. We created this lower bound by concatenating on a week-by-week basis the availability time series that had the lowest average availability of the respective 40 weeks of the same time period. The deviation value  $\widehat{cf}_{r,g,t}$  then corresponds to the difference between the reference value  $\overline{cf}_{r,g,t}$  and the lower bound of the capacity factor. An exemplary visualization of the lower bound and the reference values for solar PV in Austria is presented in Appendix B.

### 4.3 ARO Model Formulation

As described in section 3.1, the adaptive robust optimization problem is formulated as a three-level *min-max-min* problem. The deterministic problem with variables from the set  $\Phi^D$  represents the first level minimization problem. The second level of the optimization problem is defined by the uncertainty set  $\Phi^U$ . The second level maximizes the system cost by calculating the most unfortunate uncertainty realizations with respect to the variables in the set  $\Phi^U$ . The third level calculates the corrective dispatch actions after the uncertainty realization by minimizing the system costs. We introduced set  $\Phi^S$  to represent all the variables in the third level problem. This set is also referred to as the feasibility set and depends on level one and level two decisions. Our solution strategy to compute this three-level problem is to reformulate the third level problem into its dual form. By doing so, we can merge and reformulate level two, represented by set  $\Phi^U$  and level three into a single level Subproblem. As a result our ARO problem takes the following form:

$$\text{Master Problem} \quad \text{Min}_{\Phi^D} \quad (1)$$

Subject to constraint: (2)

$$GEN_{pv,t} \leq CAP_{r,pv} \cdot \overline{cf}_{pv,t}^M : \mu_{pv,t}^R, \forall pv(r), t \quad (3a)$$

$$GEN_{wind,t} \leq CAP_{wind} \cdot \overline{cf}_{wind,t}^M : \mu_{wind,t}^R, \forall wind(r), t \quad (4a)$$

Subject to constraint: (5)-(29)

$$\text{Subproblem} \quad \text{Max}_{\Phi^U \Phi^S} \quad (33)$$

$$\begin{aligned} & \sum_{n,t} \lambda_{n,t} \cdot dem_{n,t} + \sum_{c,t} -\mu_{c,t}^{conv} \cdot \overline{cap}_c + \sum_{pv,t} -\mu_{pv,t}^R \cdot (\overline{sub}_{pv}^{REN} \cdot \widehat{cf}_{pv,t}) + \phi_{pv,t}^{aux} \cdot (\overline{sub}_{pv}^{REN} \cdot \widehat{cf}_{pv,t}) \\ & + \sum_{wind,t} -\mu_{wind,t}^R \cdot (\overline{sub}_{wind}^{REN} \cdot \widehat{cf}_{wind,t}) + \phi_{wind,t}^{aux} \cdot (\overline{sub}_{wind}^{REN} \cdot \widehat{cf}_{wind,t}) \\ & + \sum_{ror,t} -\mu_{ror,t}^{ROR} \cdot \overline{cap}_{ror} + \sum_{rsv,t} -\mu_{rsv,t}^{RSV} \cdot (\overline{cap}_{rsv} \cdot af_{rsv,t}) \\ & + \sum_{psp,t} -\mu_{psp,t}^{DIS} \cdot \overline{cap}_{psp} - \mu_{psp,t}^{CH} \cdot \overline{cap}_{psp} - \mu_{PSP,t}^{CAP} \cdot (\overline{cap}_{psp} \cdot csf_{psp}) \\ & + \sum_{psp,t=1} \phi_{PSP,t=1}^{LVL} \cdot \frac{\overline{cap}_{psp} \cdot csf_{psp}}{2} \\ & + \sum_{b,t} -\mu_{b,t}^{DB} \cdot \overline{sub}_b^{INV} - \mu_{b,t}^{CB} \cdot \overline{sub}_b^{INV} - \mu_{b,t}^{CAPB} \cdot \overline{sub}_b^{STOR} \\ & + \sum_{h,t} -\mu_{h,t}^{OCGT} \cdot \overline{sub}_h^{OCGT} - \mu_{h,t}^{EL} \cdot \overline{sub}_h^{EL} - \mu_{h,t}^{CAPH} \cdot \overline{sub}_h^{STOR} \\ & + \sum_{n,t} -\mu_{n,t}^{LS1} \cdot (dem_{n,t} \cdot f^{L1}) + \sum_{n,t} -\mu_{n,t}^{LS2} \cdot (dem_{n,t} \cdot f^{L2}) \\ & + \sum_{n,t} -\mu_{n,t}^{LS3} \cdot (dem_{n,t} \cdot f^{L3}) + \sum_{l,t} -\underline{\mu}_{l,t}^L \cdot \overline{sub}_l^{Line} + \sum_{l,t} -\overline{\mu}_{l,t}^L \cdot \overline{sub}_l^{Line} \end{aligned}$$

$$\overline{cf}_{pv,g,t} = \widetilde{cf}_{pv,g,t} - \sum_{p \in P(t)} Z_{pv,g,p} \cdot \widehat{cf}_{pv,g,t} \quad \forall pv(r), \forall g, \forall t, \forall p \quad (34)$$

$$\overline{cf}_{wind,g,t} = \widetilde{cf}_{wind,g,t} - \sum_{p \in P(t)} Z_{wind,g,p} \cdot \widehat{cf}_{wind,g,t} \quad \forall wind(r), \forall g, \forall t, \forall p \quad (35)$$

$$\sum_{g \in G} Z_{pv,g,p} \leq \Gamma_{pv,p} \quad \forall pv(r), \forall p \quad (36)$$

$$\sum_{g \in G} Z_{wind,g,p} \leq \Gamma_{wind,p} \quad \forall wind(r), \forall p \quad (37)$$

$$\lambda_{n,t} - \mu_{c,t}^{Conv} \leq 0, \quad \forall n, \forall c, \forall t \quad (38)$$

$$\lambda_{n,t} - \mu_{pv,t}^R \leq 0, \quad \forall n, \forall pv(r), \forall t \quad (39)$$

$$\lambda_{n,t} - \mu_{wind,t}^R \leq 0, \quad \forall n, \forall wind(r), \forall t \quad (40)$$

$$\lambda_{n,t} - \mu_{ror,t}^{ROR} \leq 0, \quad \forall n, \forall ror, \forall t \quad (41)$$

$$\lambda_{n,t} - \mu_{rsv,t}^{RSV} \leq 0, \quad \forall n, \forall rsv, \forall t \quad (42)$$

$$\lambda_{n,t} - \phi_{PSP,t}^{LVL} - \mu_{PSP,t}^{DIS} \leq 0, \quad \forall n, \forall psp, \forall t \quad (43)$$

$$-\lambda_{n,t} + \phi_{PSP,t}^{LVL} \cdot \sigma_{psp} - \mu_{psp,t}^{CH} \leq 0, \quad \forall n, \forall psp, \forall t \quad (44)$$

$$\phi_{PSP,t}^{LVL} - \phi_{PSP,t-1}^{LVL} - \mu_{PSP,t}^{CAP} + \underline{\mu}_{PSP,t}^{CAP} = 0, \quad \forall psp, \forall t \quad (45)$$

$$\phi_{PSP,t=1}^{LVL} - \mu_{PSP,t=1}^{CAP} + \underline{\mu}_{PSP,t=1}^{CAP} = 0, \quad \forall psp \quad (46)$$

$$\lambda_{n,t} - \phi_{b,t}^{LVLB} - \mu_{b,t}^{DB} \leq 0, \quad \forall n, \forall b, \forall t \quad (47)$$

$$-\lambda_{n,t} + \phi_{b,t}^{LVLB} \cdot \sigma_b - \mu_{b,t}^{CB} \leq 0, \quad \forall n, \forall b, \forall t \quad (48)$$

$$-\phi_{b,t}^{LVLB} + \phi_{b,t+1}^{LVLB} - \mu_{b,t}^{CAPB} + \underline{\mu}_{b,t}^{CAPB} = 0, \quad \forall b, \forall t \in T \setminus \{t_{last}\} \quad (49)$$

$$-\phi_{b,t}^{LVLB} - \mu_{b,t}^{CAPB} + \underline{\mu}_{b,t}^{CAPB} = 0, \quad \forall b, \forall t_{last} \quad (50)$$

$$\lambda_{n,t} - \frac{\phi_{h,t}^{LVLH}}{\sigma_h^{OCGT}} - \mu_{h,t}^{OCGT} \leq 0, \quad \forall n, \forall h, \forall t \quad (51)$$

$$-\lambda_{n,t} + \phi_{h,t}^{LVLH} \cdot \sigma_h^{EL} - \mu_{h,t}^{EL} \leq 0, \quad \forall n, \forall h, \forall t \quad (52)$$

$$-\phi_{h,t}^{LVLH} + \phi_{h,t+1}^{LVLH} - \mu_{h,t}^{CAPH} + \underline{\mu}_{h,t}^{CAPH} = 0, \quad \forall h, \forall t \in T \setminus \{t_{last}\} \quad (53)$$

$$-\phi_{h,t}^{LVLH} - \mu_{h,t}^{CAPH} + \underline{\mu}_{h,t}^{CAPH} = 0, \quad \forall h, \forall t_{last} \quad (54)$$

$$\lambda_{n,t} - \mu_{n,t}^{LS1} \leq sc_n^{LS1}, \quad \forall n, \forall t \quad (55)$$

$$\lambda_{n,t} - \mu_{n,t}^{LS2} \leq sc_n^{LS2}, \quad \forall n, \forall t \quad (56)$$

$$\lambda_{n,t} - \mu_{n,t}^{LS3} \leq sc_n^{LS3}, \quad \forall n, \forall t \quad (57)$$

$$-\lambda_{s(l)} + \lambda_{r(l)} - \overline{\mu}_{l,t}^L + \underline{\mu}_{l,t}^L + \phi_{l,t}^L = 0, \quad \forall t, \forall l \in AC(l) \quad (58)$$

$$-\lambda_{s(l)} + \lambda_{r(l)} - \overline{\mu}_{l,t}^L + \underline{\mu}_{l,t}^L = 0, \quad \forall t, \forall l \in DC(l) \quad (59)$$

$$\sum_{s(l)} (sus_l \cdot \phi_{l,t}^L) - \sum_{r(l)} (sus_l \cdot \phi_{l,t}^L) - \underline{\mu}_{n,t}^N + \overline{\mu}_{n,t}^N = 0, \quad \forall n, \forall t \quad (60)$$

$$\sum_{s(l)} (sus_l \cdot \phi_{l,t}^L) - \sum_{r(l)} (sus_l \cdot \phi_{l,t}^L) - \underline{\mu}_{n,t}^N + \overline{\mu}_{n,t}^N + \epsilon^{ref} = 0, \quad \forall n, \forall t \quad (61)$$

$$(-M) \cdot Z_{pv,g,p} \leq \phi_{pv,t}^{aux} \leq M \cdot Z_{pv,g,p}, \quad \forall pv(r), \forall g, \forall p, \forall t \quad (62)$$

$$(-M) \cdot (1 - Z_{pv,g,p}) \leq \mu_{pv,t}^R - \phi_{pv,t}^{aux} \leq M \cdot (1 - Z_{pv,g,p}), \quad \forall pv(r), \forall g, \forall p, \forall t \quad (63)$$

$$(-M) \cdot Z_{wind,g,p} \leq \phi_{wind,t}^{aux} \leq M \cdot Z_{wind,g,p}, \quad \forall wind(r), \forall g, \forall p, \forall t \quad (64)$$

$$(-M) \cdot (1 - Z_{wind,g,p}) \leq \mu_{wind,t}^R - \phi_{wind,t}^{aux} \leq M \cdot (1 - Z_{wind,g,p}), \quad \forall wind(r), \forall g, \forall p, \forall t \quad (65)$$

$$\text{Positive variables: } \mu_{c,t}^{Conv}; \mu_{pv,t}^R; \mu_{wind,t}^R; \mu_{ror,t}^{ROR}; \mu_{rsv,t}^{RSV}; \mu_{psp,t}^{DIS}; \mu_{psp,t}^{CH}; \mu_{b,t}^{CAPB}; \mu_{h,t}^{EL}; \mu_{h,t}^{OCGT}; \mu_{h,t}^{CAPH}; \quad (66)$$

$$\mu_{n,t}^{LS1}; \mu_{n,t}^{LS2}; \mu_{n,t}^{LS3}; \bar{\mu}_{l,t}^L; \underline{\mu}_{l,t}^L; \bar{\mu}_{n,t}^N; \underline{\mu}_{n,t}^N; \phi_{pv,t}^{aux}; \phi_{wind,t}^{aux}$$

$$\text{Free variables: } \lambda_{n,t}; \phi_{l,t}^L; \phi_{psp,t}^{LVL}; \phi_{b,t}^{LVLB}; \phi_{h,t}^{LVLH}; \epsilon^{ref} \quad (67)$$

Note that within the formulation of the Master Problem, the renewable availability constraints (3a) and (4a) are adjusted with the new parameters  $\bar{c}f_{pv,t}^M$ ,  $\bar{c}f_{wind,t}^M$ . These parameters are determined as variables by the Subproblem which maximizes the objective function by identifying the most unfortunate realization of  $\bar{C}f_{wind,g,t}$  and  $\bar{C}f_{pv,g,t}$ , defined by Eqs. (34)-(37). The dual generation constraints of the conventional generators, the renewable generators, and the hydro generators are described by Eqs. (38)-(42). The dual storage reformulation for the pumped hydro storage is defined by Eqs. (43-46), followed by the dual battery storage formulation in Eqs. (47)-(50), and by the dual hydrogen storage formulation from Eqs. (51)-(54). The dual load shedding formulation is described by Eqs. (55)-(57), followed by the dual formulation of the transmission line flows in Eqs. (58)-(61). We use the big M constraints in Eqs. (62)-(65) and introduce the auxiliary variables  $\phi_{pv,t}^{aux}$  and  $\phi_{wind,t}^{aux}$  to replace the non-linear term in the objective function  $\mu_{pv,t}^R \cdot \bar{C}f_{pv,g,t}$  and  $\mu_{wind,t}^R \cdot \bar{C}f_{wind,g,t}$  with an equivalent linear formulation. The dual variable types are declared in Eqs. (66) and (67).

As described in section 3.3, this problem is solved with a column-constraint generation algorithm that iterates over the Master Problem and Subproblems until a predefined convergence tolerance between the two objective functions is archived. Therefore, information between the Master and the Subproblem is exchanged, as visualized in Figure 1. From the Master Problem, the generation and transmission capacity expansion decisions are transferred to the Subproblem by storing the information in the following parameter set  $\Phi^{M \rightarrow S} = \{\bar{sub}_{pv}^{REN}; \bar{sub}_{wind}^{REN}; \bar{sub}_b^{INV}; \bar{sub}_b^{STOR}; \bar{sub}_h^{OCGT}; \bar{sub}_h^{EL}; \bar{sub}_l^{STOR}; \bar{sub}_l^{Line}\}$ . The Subproblem stores the information of the renewable capacity factors worst case realizations in parameters  $\bar{c}f_{pv,t}^M$  and  $\bar{c}f_{wind,t}^M$ , and sends the information to the Master Problem, described by set  $\Phi^{S \rightarrow M} = \{\bar{C}f_{pv,g,t} \rightarrow \bar{c}f_{pv,t}^M; \bar{C}f_{wind,g,t} \rightarrow \bar{c}f_{wind,t}^M\}$ .

## 4.4 Scenario Definition

Since we examine the effect of different geographical coverages of low availability events, we investigate six different scenarios, ARO1 to ARO6, by gradually increasing the uncertainty budgets  $\Gamma_{pv}$  and  $\Gamma_{wind}$ . In simple terms, ARO specifies that N regions are affected by a low availability event for wind, and N regions are hit by a low availability event for solar PV. More formally, the integer number of the respective uncertainty budget represents the number of regions that can be affected by low solar PV or wind availability periods. Thus, the model endogenously decides in which region the availability is reduced. For example, in the ARO2 scenario, the model can set the availability of solar PV and wind to the lower bound in two regions. For instance, this could mean low solar PV availability in regions 1 and 2, and low wind availability in regions 2 and 3. In the following, we will refer to an event as a ‘‘Dunkelflaute’’ when low availability events for both solar PV and wind realized in the same region, such as region 2 in this example. The ARO6 scenario thus specifies a simultaneous Dunkelflaute all over Europe. We contrast these scenarios to a Base scenario, in which no low availability event realizes. An overview of the scenarios and their respective uncertainty budgets is provided in Table 1. Furthermore, we restrict the model to simulate weekly low solar and wind generation periods during the month of January, as this month typically aligns with when such events occur.

**Table 1** Scenarios of weather uncertainty realization potential.

Scenarios	Uncertainty Budgets	
	$\Gamma_{pv}$	$\Gamma_{wind}$
Base (average weather year)	0	0
ARO1	1	1
ARO2	2	2

ARO3	3	3
ARO4	4	4
ARO5	5	5
ARO6	6	6

## 5 MODEL RESULTS

In the following, we outline the application of the ARO framework and the results of our case study. Section 5.1 presents the iterative modeling process, with a focus on the convergence behavior of the min-max problem and the extreme event realizations. Section 5.2 presents the identified worst-case weather events and analyzes their impact on investment and generation costs. Section 5.3 examines the resulting robust, technology-specific generation mix, while Section 5.4 discusses the corresponding storage capacities for each scenario, both at the European level and disaggregated by region.

### 5.1 Iterative ARO Process – Incorporation of Uncertainty

The model endogenously stresses the specified weather regions with low solar PV or wind availability events. Therefore, it iterates over the possible realization space which includes four weeks of January and the six geographical regions. The model terminates when the gap between the primal and the dual objective value is lower than a predefined tolerance.<sup>4</sup> Figure 3 illustrates this convergence process for each ARO scenario, with the duality gap plotted on a logarithmic scale (y-axis) over the number of iterations (x-axis). The red line indicates the convergence tolerance that serves as the stopping criterion for the algorithm.

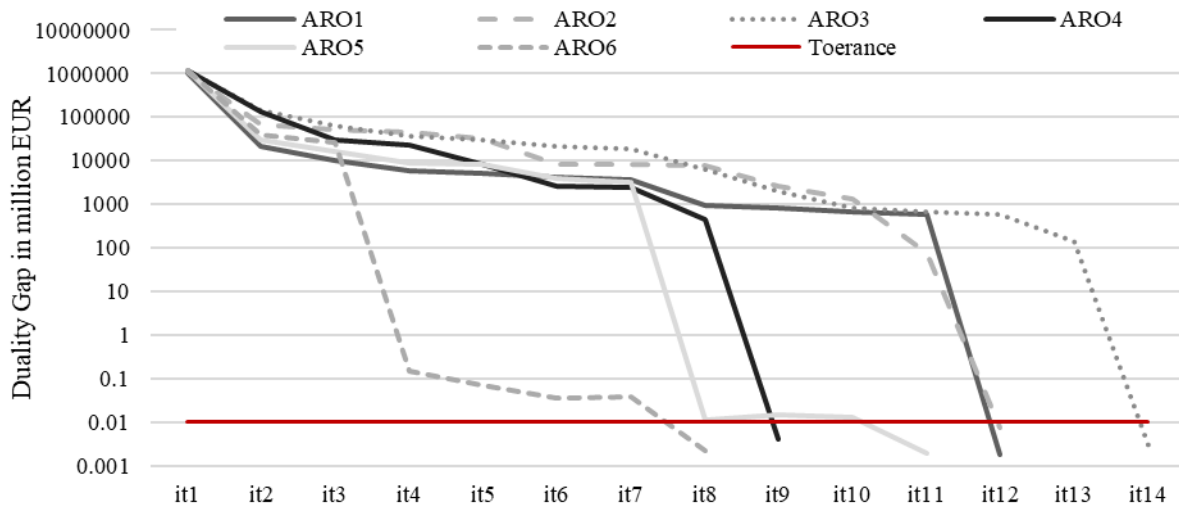


**Figure 3: Convergence Process - Development of the Duality Gap for each ARO Scenario**

The figure reveals a consistent three phase convergence progress of the ARO algorithm. In the first phase, the algorithm rapidly minimizes the duality gap up to a certain cost interval between 100 billion and 10 billion EUR. From here the second phase can be seen as saturation phase, where the min-max algorithm slowly progresses on closing the duality gap. In the third and final phase, a steep decline in the duality gap is observed, reflecting the identification of near-robust or robust capacity layout that meets the convergence criterion. As one can see, this process is different for each ARO scenario. Scenarios such as ARO1, ARO2, and ARO3 require more iterations to converge. This indicates that identifying a robust system layout in these cases requires exploring a broader set of adverse weather events before achieving convergence. The resulting extreme event realization in the last iteration is then referred to as the worst-case geographical configuration within the given uncertainty budget. Table 2 below illustrates this process in more detail.

<sup>4</sup> For our case the threshold is less than 0.000001% of the objective function value.

For each scenario (ARO1-ARO6), the table indicates the iteration (it1-it14), region (1-6), and time period (four weeks in January) for which the extreme event realization can occur. The colored cells highlight the times and regions at which the capacity factor time series is reduced to their historical lower bounds—yellow for solar PV, blue for onshore and offshore wind, and black for both technologies simultaneously (Dunkelflaute). For example, in scenario ARO1, the model explores extreme event realization in 12 iterations, starting with low solar PV availability in week 4 of January in Region 4 and reduced wind availability in Region 5. Subsequent iterations test other combinations, such as simultaneous low solar PV and wind availability in week 2 in Region 3. The red-framed cells in the table indicate the iteration at which the model converges, presenting our final worst-case solution. Note that the capacity layout for the resulting system is robust towards all combinations possible, not only against the ones tested. This is because not all combinations of low availability events will automatically result in a case that is difficult to mitigate for the system. Occasionally, the same extreme event reappears across iterations - e.g., in ARO1, the Dunkelflaute in Region 3 during week 2 is identified in both iteration 2 and the final iteration 12. This occurs because the model retains all previous iterations when looking for the worst-case event and adopts the generation and transmission expansion decisions accordingly. Consequently, the memory of the model grows with each iteration. Thus, identifying a possible worst-case event in iteration 3 is easier than in iteration 12. In some cases, after evaluating the previous possibilities, the model reconfirms the same event again to be a possible worst case. This means that the generation and transmission expansion adoptions made lead the model to find the event realization as only possibility, where the primal objective equals the dual objective. All other uncertainty realizations are automatically excluded, and the model converges.

As the uncertainty budget increases from the ARO1 to the ARO6 scenario, more regions are affected either simultaneously or even at different times. Overall, the model finds simultaneous extreme events to be harder to mitigate. For instance, in scenario ARO4, iteration 1 features low availability in both week 3 and week 4. In subsequent iterations, only simultaneous low availability periods occur, with varying low availability events between the affected regions. Furthermore, one can see that the number of cells that show both technologies affected (Dunkelflaute) increases with higher uncertainty budget.

**Table 2: Iterative uncertainty selection process of the model for each scenario**

Iteration	Week January	ARO1		ARO2		ARO3		ARO4		ARO5		ARO6								
		Regions		Regions		Regions		Regions		Regions		Regions								
		1	2	3	4	5	6	1	2	3	4	5	6	1	2	3	4	5	6	
it1	1																			
	2																			
	3																			
	4																			
it2	1																			
	2																			
	3																			
	4																			
it3	1																			
	2																			
	3																			
	4																			
it4	1																			
	2																			
	3																			
	4																			
it5	1																			
	2																			
	3																			
	4																			
it6	1																			
	2																			
	3																			
	4																			
it7	1																			
	2																			
	3																			
	4																			
it8	1																			
	2																			
	3																			



The lower part of Figure 4 shows the progression of total system costs (i.e., the model's objective value), which includes annual investment and generation costs as defined in Equation (1) in Subsection 4.1. It also displays the average electricity cost per scenario. In the Base scenario, total system costs amount to €151 billion, with an average electricity cost of €51/MWh. In ARO1, costs rise moderately by 9 %, suggesting that the integrated European system can efficiently absorb localized extreme events. However, as more regions experience low availability, system costs increase rapidly: in ARO2, costs reach €199 billion (+31 %) with €66/MWh on average; in ARO3, they rise to €228 billion (+50 %); in ARO4, to €245 billion (+62 %); and in ARO5, to €256 billion (+70 %) with an average cost of €85/MWh. The increase in ARO6 is marginal, reaching €258.5 billion (+71 %) and €86/MWh on average. This steep rise followed by a plateau indicates a nonlinear system response, where early regional shocks are manageable, but broader events quickly exhaust cost-effective adaptation measures.

The regional cost shares shown in Figure 4 further illustrate how the system cost burden is distributed. Across all scenarios, Regions 3, 5, and 6 contribute the most to total system costs. Nearly all regions, except Region 6, approximately double their costs from the Base to the ARO6 scenario due to shifts in their generation mix. However, the sensitivity to scenario severity varies by region. In the early scenarios, cost increases are driven mainly by Region 6, while other regions see only modest changes. From ARO3 onward, Region 6's costs begin to decline, while Regions 1, 3, and 5 show substantial increases. This pattern suggests that Region 6 is particularly vulnerable to smaller-scale Dunkelflaute events, where it must absorb the renewable shortfall on its own. As more regions are affected in later scenarios, the compensation burden is redistributed, alleviating pressure on Region 6 and helping stabilize its supply.

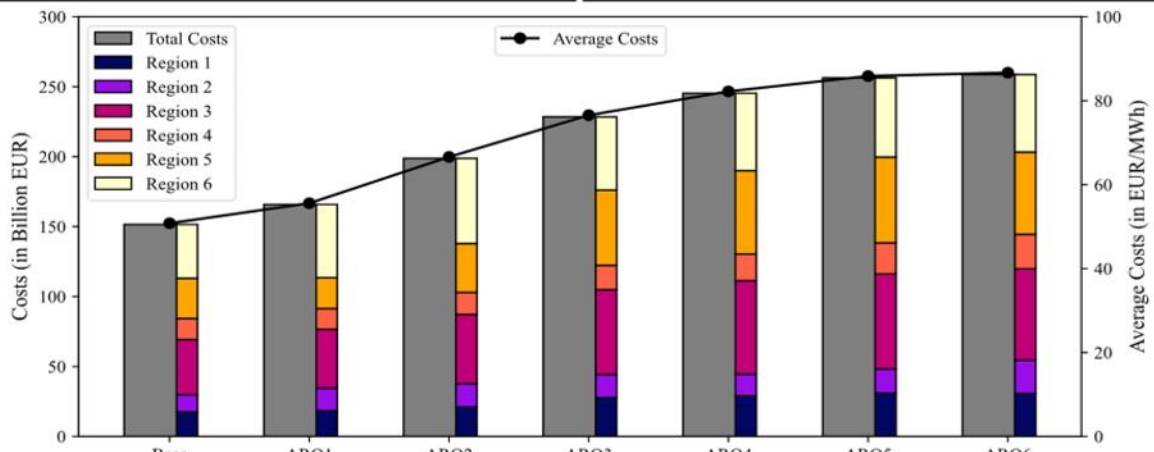
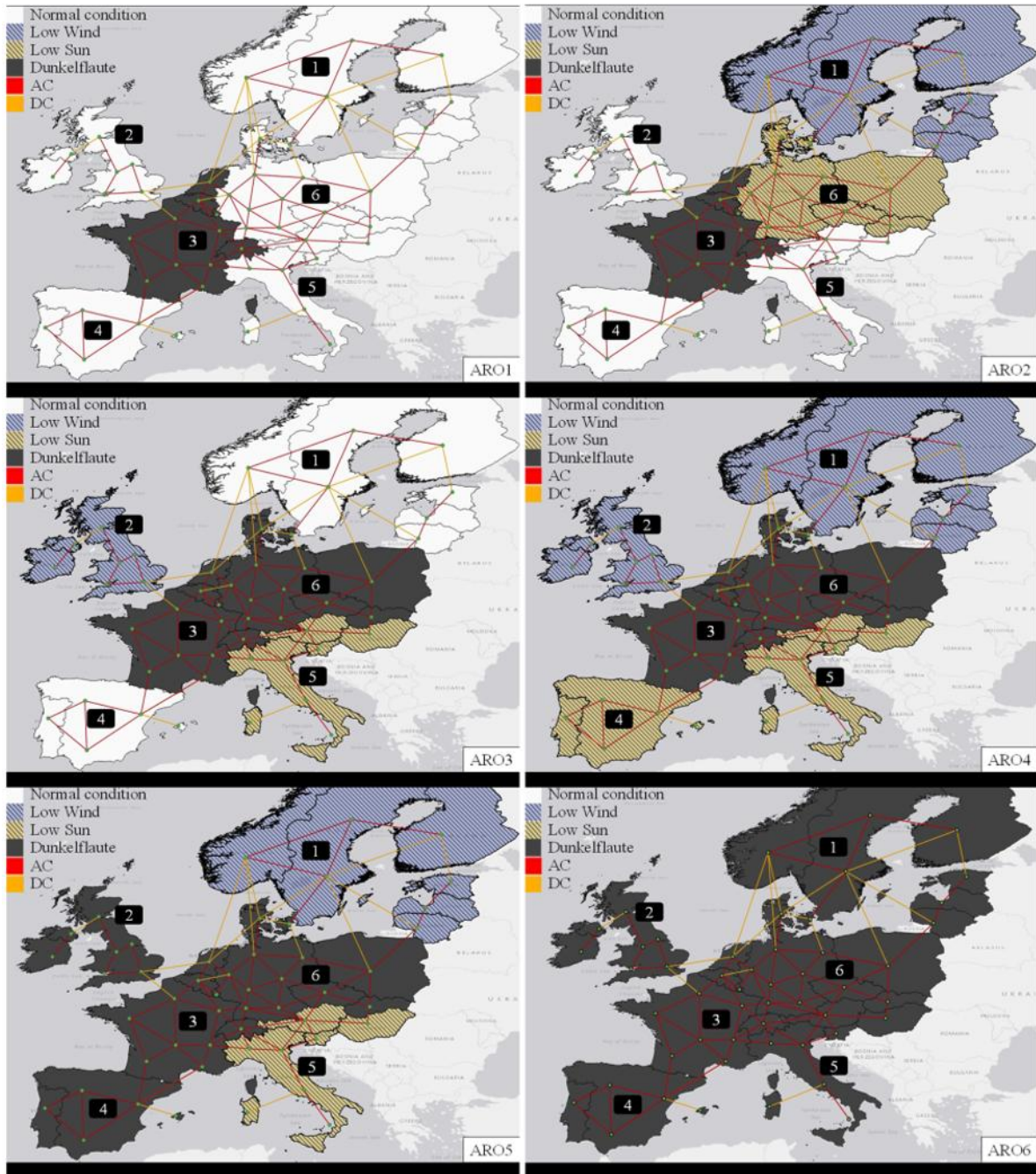


**Figure 4.** Scenario specific worst case regional weather realizations, maps for ARO1, ARO2, ARO3, ARO4, ARO5, ARO6, and system costs with regional shares and average electricity costs.

Figure 5 reveals the trends in technology-specific investments. Onshore wind appears consistently across all regions, while significant solar PV deployment is concentrated in Regions 4 and 5 and, depending on the scenario, also in Regions 3 and 6. In particular, Regions 3 and 6 show more prominent solar PV investments in low-coverage scenarios (ARO1–ARO3), which decline as the number of affected regions increases in higher-coverage scenarios (ARO4–ARO5).

Additionally, we observe a substantial increase in investment cost for long-term hydrogen storage and load shedding as more regions are impacted by low availability. Hydrogen storage investments become significant starting in ARO2, especially in Regions 1, 3, 5, and 6. By ARO6, hydrogen storage accounts for 19%–25% of the regional system costs. Load shedding also becomes a relevant measure from ARO2 onward, with the model increasingly relying on both storage technologies and demand curtailment to meet the final megawatts of residual demand during extreme events.

These findings demonstrate that the optimal robust investment mix is shaped not only by the severity of *Dunkelflaute* events but also by their regional resource endowments. In particular, long-term storage technologies emerge as critical components of the robust solution once extreme events affect a broader portion of the system.

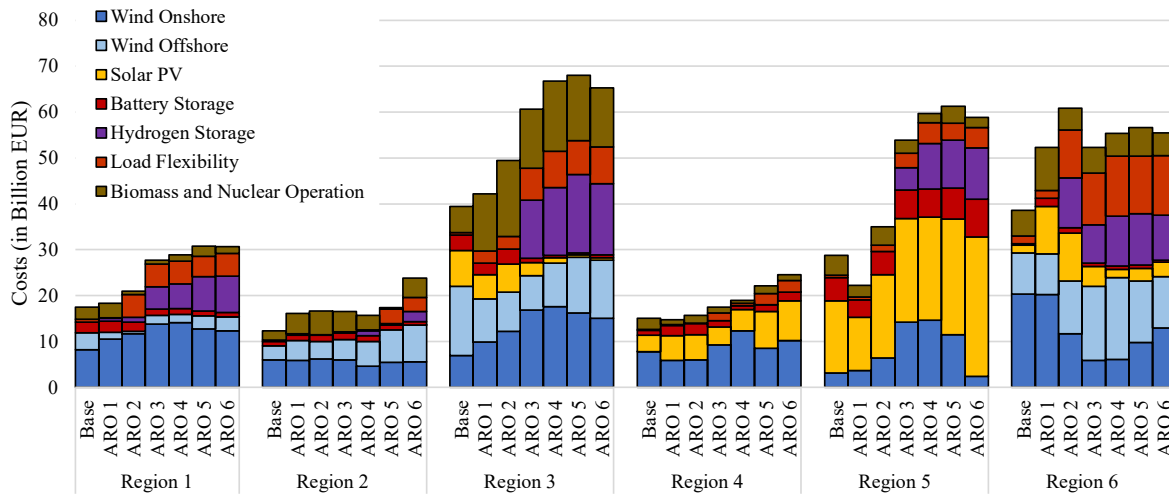


Figure 5. Regional and scenario-specific electricity investment, generation, and load shedding costs.

### 5.3 Installed Capacity and Regional Generation Mix

Figure 6 depicts the scenario-specific installed capacities for each technology, aggregated across Europe. Despite its modest share in total system costs, solar PV comprises the largest share of installed capacity, reaching up to 50% across all scenarios. Wind power represents the second-largest share, with onshore wind dominating over offshore. Battery inverters form the third-largest component of installed capacity. Investments in battery inverters increase notably when one or two regions are affected by low availability events but decline and stabilize as more regions become impacted. Overall, battery deployment closely follows the pattern of solar PV investments.

In line with the cost trend, the installed capacities of hydrogen technologies, specifically electrolyzers (for charging) and H<sub>2</sub>-fired OCGTs (for discharging), become significant from ARO3 onwards, with 66 GW of electrolyzer and 45 GW of OCGT capacity. These capacities continue to grow through ARO6, reaching approximately 98 GW of electrolyzers and 70 GW of OCGTs, together accounting for around 6% of total installed capacity. This trend reinforces the role of long-term hydrogen storage as a preferred solution for handling large-scale *Dunkelflaute* events.

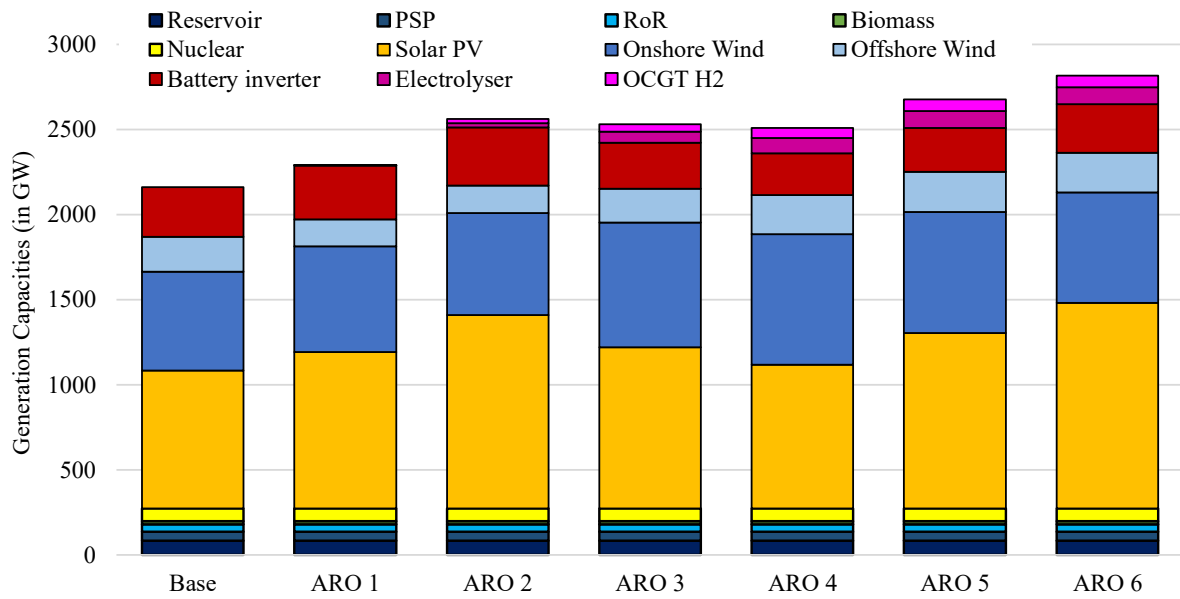


Figure 6. Scenario-specific technology capacity mix.

Figure 7 presents the regionally differentiated, scenario-specific annual electricity generation (in TWh), alongside regional electricity demand indicated by red dotted lines. When a region's total generation exceeds this line, it functions as a net exporter. Electricity generation is dominated by wind power in most regions, while solar PV plays a more prominent role in Southern Europe. Most regions are either net exporters or nearly self-sufficient, with the exception of Region 6, where electricity demand significantly exceeds domestic generation.

When only Region 3 is affected by low availability (e.g., in ARO1), Region 6 responds with increased domestic generation investment. However, as additional regions are impacted, Region 6 reduces its investment and maintains a relatively stable generation level.

Although hydrogen technologies account for a substantial share of total system costs, their contribution to electricity generation remains modest. A similar pattern is seen with load shedding, which stays below 1% of total generation in all scenarios. This stark contrast between cost and energy output highlights the high expense of maintaining backup capacity to safeguard the system during extreme low availability periods. Identifying cost-effective, large-scale backup solutions remains a critical challenge for reducing total system costs. Detailed regional and scenario-specific analysis is provided in Appendix D.

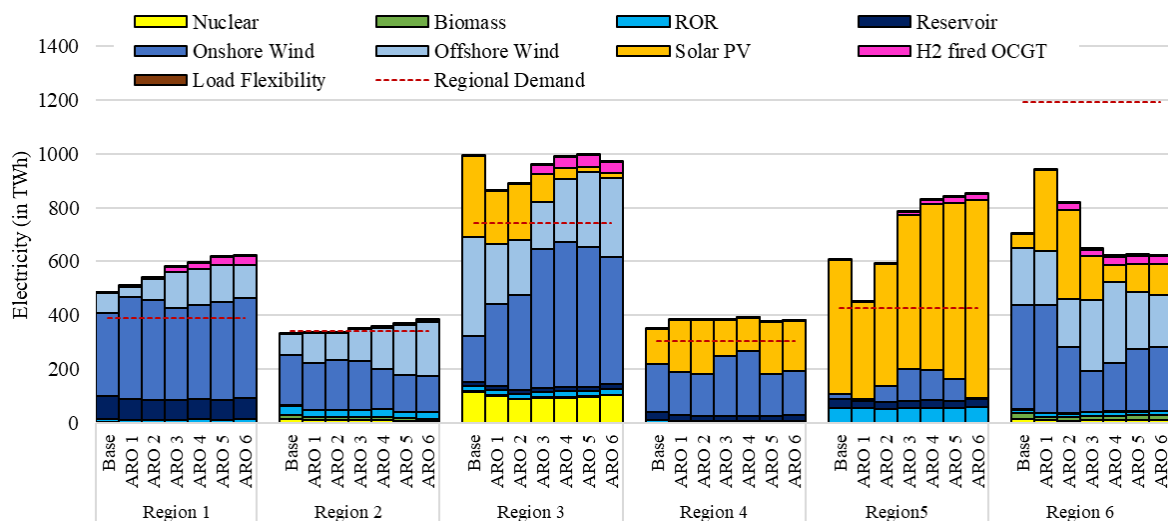
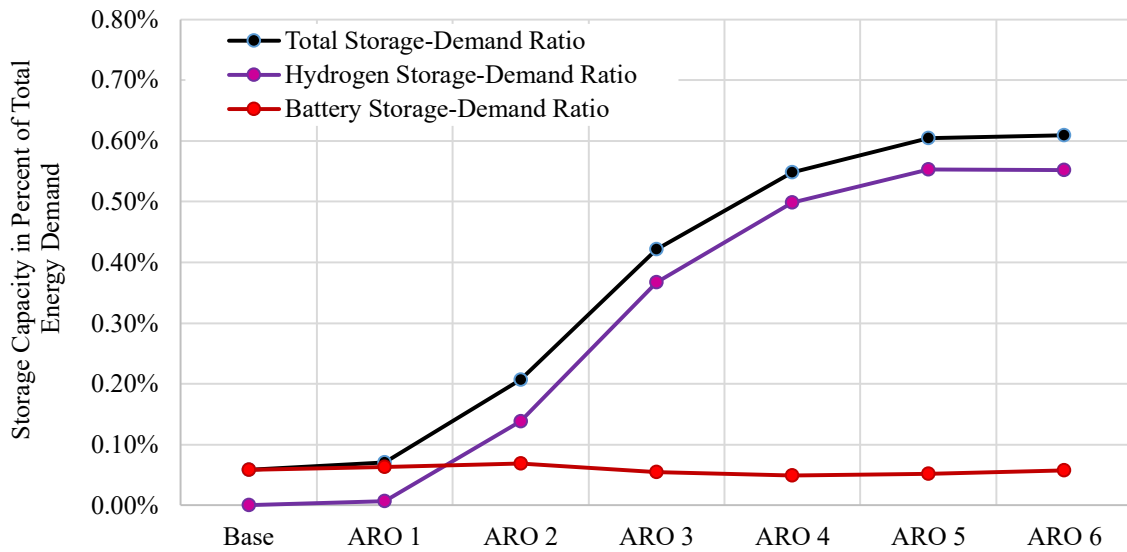


Figure 7. Regional generation mix in relation to the regional demand.

## 5.4 Storage Capacity Expansion

Figure 8 illustrates the storage-demand ratio across scenarios, breaking down total storage into hydrogen and battery storage as a share of annual energy demand. This metric enables comparison of storage requirements across systems and serves as a

proxy for the flexibility storage provides to the energy system. For more detailed insights on this metric, the interested reader is referred to Zerrahn et al. (2018). We use different colors to represent different storages, red color for short-term battery storage, and purple color for long-term hydrogen storage.



**Figure 8.** Scenario and technology specific storage capacity demand ratio.

The figure shows that the total storage-demand ratio falls between 0.08 % for the Base and 0.7 % for the ARO6 scenario. The ratio significantly increases from scenario ARO2 onwards. This increase is related to the expansion of long-term hydrogen storage. The hydrogen storage capacity increases strongly in the ARO2 to ARO4 scenarios compared to the Base scenario while it is the same in ARO5 and ARO6. On the contrary, the battery storage capacity remains almost constant throughout all scenarios. To quantify the regional contribution of the storage capacity expansion, Figure 9 depicts the regional storage-demand ratio on the primary as well as the total regional storage capacity on the secondary Y-axis.

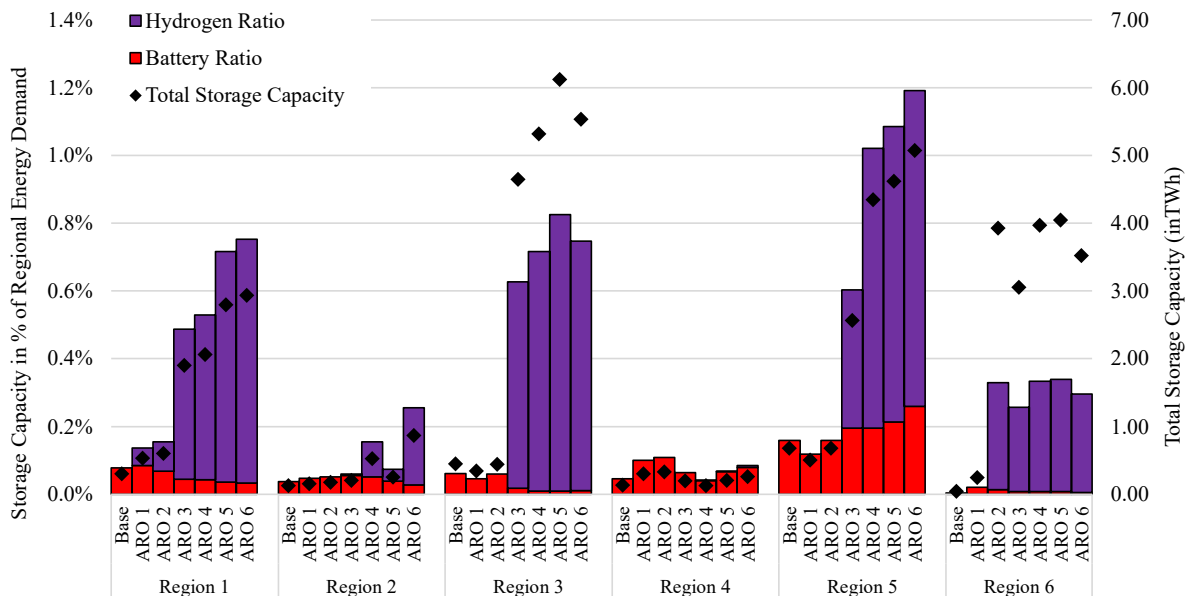


**Figure 9.** Regional storage-demand ratio plotted with stacked bars for battery storage capacity and hydrogen storage capacity on the primary axis, regional storage capacity plotted with black markers on the secondary axis.

The diagram reflects the previous finding that in the first two ARO scenarios most of the storage capacity in each region, but Region 6, comes from battery systems. As solar PV generation in Region 3 and Region 5 plays a major role, so does the battery storage capacity. Starting from the ARO2 scenario, the hydrogen storage expansion becomes significant, mainly driven by expansion in Region 1 and Region 6. Notably, in the ARO2 scenario, Region 6 significantly increases its

hydrogen storage capacity, constructing more storage capacity (4 TWh) than all the other regions combined. However, from the ARO3 scenario Region 1, Region 4 and Region 5 are catching up, making Region 3 the region with the highest installed hydrogen storage capacity. For the ARO 6 scenario, the hydrogen storage capacity for the system totals 16.5 TWh and the battery storage capacity 1.7 TWh. To evaluate the role of storage in ensuring system stability, Table 3 presents the installed H<sub>2</sub>-fired OCGT capacity and the maximum hydrogen storage discharge duration (in days) for the ARO6 scenario as a representative worst-case example.

**Table 3** Maximum discharging capacity and duration of long-term storage in the ARO6 scenario.

Region	Region 1	Region 2	Region 3	Region 4	Region 5	Region 6
H <sub>2</sub> fired OCGT in GW	11.8	4.0	24.1	0.1	16.5	13.9
Duration in days	5.8	4.8	5.5	4.7	5.9	6.1

The table indicates that hydrogen storage is dimensioned to cover between four and six days of demand, aligning closely with the modeled seven-day extreme events. The capacities of both hydrogen storage and OCGT plants are optimized accordingly. Region 3 and Region 5 install the highest levels of OCGT capacity, enabling them to support not only their own loads but also partially cover Region 6 during extreme events. This finding is evaluated in more detail in Appendix D.

These results highlight how worst-case events identified by the model shape the regional demand for long-duration storage, revealing the cost sensitivity of different regions under stress. The earlier hydrogen storage appears in the optimal capacity mix, the more exposed a region is to extreme events—suggesting that lower-cost options such as load flexibility, transmission, or renewable generation expansion have already been exhausted. An alternative - expanding other firm capacity like oil power plants or carbon-neutral nuclear power plants to cover the period - remains outside the scope of this analysis.

## 6 DISCUSSION AND CONCLUSION

In this study, we developed a capacity expansion model for Europe based on an ARO framework. A key strength of ARO is its sequential decision-making structure, which enables the model to adapt to weather-related uncertainties and endogenously identify the most severe regional Dunkelflaute events. Methodologically, we show how multiple extreme weather realizations, up to 14 in the ARO3 scenario, can be incorporated as endogenous uncertainty scenarios within a single optimization run.

Our results reveal a nonlinear cost response as the geographical scope of low availability events increases. Compared to the baseline scenario (€151.6 billion), system costs rise moderately under localized shocks (+9% in ARO1), but increase sharply when broader impacts are considered (+31% in ARO2, +51% in ARO3). As more regions are affected, marginal cost increases taper off: +62 % in ARO4, +69 % in ARO5, and +71 % in ARO6. The small difference between ARO5 and ARO6 indicates that once most of Europe is affected by Dunkelflaute events, additional coverage has limited impact on system cost. These findings underscore the importance of accounting for widespread regional weather events when designing a robust electricity system for the entire Europe.

Comparison with previous studies shows that ARO1 (+9%) aligns closely with deterministic models such as Gøtske et al. (2024) and Grochowicz et al. (2024b), while ARO2 (+31%) yields results similar to those of Plaga and Bertsch (2022), who employ robust optimization. The significantly higher costs observed in ARO3 and beyond likely stem from our model design, which combines multiple worst-case events and enforces a strict carbon cap, excluding other low-carbon backup options such as nuclear power, and incorporates relatively high costs for load shedding. While these assumptions may yield conservative estimates, they enable us to explore the upper bounds of system cost escalation and to identify the technologies required to hedge against large-scale Dunkelflaute events across Europe.

Another key insight is the shift in optimal system configuration as the scale of the extreme event grows. For small-scale events (ARO1, ARO2), expanding renewables, batteries, and transmission capacity is cost-effective. But as interregional balancing becomes constrained by widespread weather events, long-term hydrogen storage becomes essential. Although hydrogen accounts for a large share of system costs, its actual contribution to electricity generation remains modest. Likewise, load shedding remains under 1% of total generation in all scenarios but still significantly drives system costs, highlighting the need for affordable, large-scale backup capacity.

At the regional level, the ARO model consistently identifies Central European regions, particularly Regions 3 and 6, as critical. Region 6, which includes major demand centers like Germany, relies on imports from Region 3, a strong renewable producer. When either is affected by low availability, the cost of reconfiguring the system increases substantially. Peripheral regions

(e.g., Regions 1, 2, 4, and 5) are less frequently selected for extreme events but still face high adaptation costs when central regions are impacted, often overbuilding infrastructure to maintain system balance.

These findings underscore the strategic importance of Central Europe in maintaining system-wide resilience and highlight the broader need for coordinated European energy policy. To avoid future fragmentation driven by national priorities, the EU must proactively support investment in renewables and storage in high-potential regions, strengthen transmission links, and incentivize system resilience near key demand hubs.

A key limitation of this study lies in the representation of weather data. First, we use a synthetic average weather year rather than a historical one for the Base scenario. While this approach captures representative renewable generation patterns, it may not fully reflect the variability and temporal extremes found in real-world data. Second, to reduce computational complexity, we apply a time series reduction technique using a four-hour moving average. This smoothing may underestimate the intensity and frequency of short-lived extreme events. Third, the model assumes static, predefined weather regions for the realization of extreme events, which does not reflect the continuous and dynamic nature of real weather systems. In reality, low availability conditions can span irregular and shifting geographical areas. These assumptions may lead to an underestimation of required storage in the Base scenario and an overestimation of extreme event impacts in the ARO scenarios. Additional model limitations include fixed capacities for firm generation technologies (e.g., nuclear), which are based on current levels or policy targets, and constraints on transmission expansion. Allowing these capacities to expand endogenously or without limits could lead to different investment strategies.

## 7 REFERENCES

- Baringo, L., Boffino, L., Oggioni, G., 2020. Robust expansion planning of a distribution system with electric vehicles, storage and renewable units. *Applied Energy* 265, 114679. <https://doi.org/10.1016/j.apenergy.2020.114679>
- Baringo, L., Rahimiyan, M., 2020. *Virtual Power Plants and Electricity Markets: Decision Making Under Uncertainty*. Springer International Publishing, Cham. <https://doi.org/10.1007/978-3-030-47602-1>
- Bertsimas, D., Litvinov, E., Sun, X.A., Zhao, J., Zheng, T., 2013. Adaptive Robust Optimization for the Security Constrained Unit Commitment Problem. *IEEE Trans. Power Syst.* 28, 52–63. <https://doi.org/10.1109/TPWRS.2012.2205021>
- Bertsimas, D., Sim, M., 2004. The Price of Robustness. *Operations Research* 52, 35–53. <https://doi.org/10.1287/opre.1030.0065>
- Birge, J.R., Louveaux, F., 2011. *Introduction to Stochastic Programming*, Springer Series in Operations Research and Financial Engineering. Springer New York, New York, NY. <https://doi.org/10.1007/978-1-4614-0237-4>
- Bloomfield, Hannah C., Brayshaw, D.J., Charlton-Perez, A.J., 2020. Characterizing the winter meteorological drivers of the European electricity system using targeted circulation types. *Meteorological Applications* 27, e1858. <https://doi.org/10.1002/met.1858>
- Bloomfield, H. C., Suitters, C.C., Drew, D.R., 2020. Meteorological Drivers of European Power System Stress. *Journal of Renewable Energy* 2020, e5481010. <https://doi.org/10.1155/2020/5481010>
- Brown, T., Schlachtberger, D., Kies, A., Schramm, S., Greiner, M., 2018. Synergies of sector coupling and transmission reinforcement in a cost-optimised, highly renewable European energy system. *Energy* 160, 720–739. <https://doi.org/10.1016/j.energy.2018.06.222>
- Brunner, C., Misconel, S., Hauser, P., Möst, D., 2025. To what extent can flexibility options reduce the need for hydrogen backup power plants? *Energy Policy* 201, 114551. <https://doi.org/10.1016/j.enpol.2025.114551>
- Caglayan, D.G., Heinrichs, H.U., Robinius, M., Stolten, D., 2021. Robust design of a future 100% renewable european energy supply system with hydrogen infrastructure. *International Journal of Hydrogen Energy, HYDROGEN ENERGY SYSTEMS* 46, 29376–29390. <https://doi.org/10.1016/j.ijhydene.2020.12.197>
- Conejo, A.J., Baringo Morales, L., Kazempour, S.J., Siddiqui, A.S., 2016. *Investment in Electricity Generation and Transmission*. Springer International Publishing, Cham. <https://doi.org/10.1007/978-3-319-29501-5>
- Conejo, A.J., Wu, X., 2022. Robust optimization in power systems: a tutorial overview. *Optim Eng* 23, 2051–2073. <https://doi.org/10.1007/s11081-021-09667-3>
- Davis, S.J., Lewis, N.S., Shaner, M., Aggarwal, S., Arent, D., Azevedo, I.L., Benson, S.M., Bradley, T., Brouwer, J., Chiang, Y.-M., Clack, C.T.M., Cohen, A., Doig, S., Edmonds, J., Fennell, P., Field, C.B., Hannegan, B., Hodge, B.-M., Hoffert, M.I., Ingersoll, E., Jaramillo, P., Lackner, K.S., Mach, K.J., Mastrandrea, M., Ogden, J., Peterson, P.F., Sanchez, D.L., Sperling, D., Stagner, J., Trancik, J.E., Yang, C.-J., Caldeira, K., 2018. Net-zero emissions energy systems. *Science* 360, eaas9793. <https://doi.org/10.1126/science.aas9793>

- Gøtske, E.K., Andresen, G.B., Neumann, F., Victoria, M., 2024. Designing a sector-coupled European energy system robust to 60 years of historical weather data. *Nat Commun* 15, 10680. <https://doi.org/10.1038/s41467-024-54853-3>
- Grochowicz, A., Greevenbroek, K. van, Benth, F.E., Zeyringer, M., 2023. Intersecting near-optimal spaces: European power systems with more resilience to weather variability. *Energy Economics* 106496. <https://doi.org/10.1016/j.eneco.2022.106496>
- Grochowicz, A., van Greevenbroek, K., Bloomfield, H.C., 2024a. Using power system modelling outputs to identify weather-induced extreme events in highly renewable systems. *Environ. Res. Lett.* 19, 054038. <https://doi.org/10.1088/1748-9326/ad374a>
- Grochowicz, A., Van Greevenbroek, K., Bloomfield, H.C., 2024b. Using power system modelling outputs to identify weather-induced extreme events in highly renewable systems. *Environ. Res. Lett.* 19, 054038. <https://doi.org/10.1088/1748-9326/ad374a>
- Jabr, R.A., 2013. Robust Transmission Network Expansion Planning With Uncertain Renewable Generation and Loads. *IEEE Trans. Power Syst.* 28, 4558–4567. <https://doi.org/10.1109/TPWRS.2013.2267058>
- Jurasz, J., Mikulik, J., Dąbek, P.B., Guezgouz, M., Kaźmierczak, B., 2021. Complementarity and ‘Resource Droughts’ of Solar and Wind Energy in Poland: An ERA5-Based Analysis. *Energies* 14, 1118. <https://doi.org/10.3390/en14041118>
- Li, B., Basu, S., Watson, S.J., Russchenberg, H.W.J., 2021a. A Brief Climatology of Dunkelflaute Events over and Surrounding the North and Baltic Sea Areas. *Energies* 14, 6508. <https://doi.org/10.3390/en14206508>
- Li, B., Basu, S., Watson, S.J., Russchenberg, H.W.J., 2021b. Mesoscale modeling of a “Dunkelflaute” event. *Wind Energy* 24, 5–23. <https://doi.org/10.1002/we.2554>
- Li, B., Basu, S., Watson, S.J., Russchenberg, H.W.J., 2020. Quantifying the Predictability of a ‘Dunkelflaute’ Event by Utilizing a Mesoscale Model. *J. Phys.: Conf. Ser.* 1618, 062042. <https://doi.org/10.1088/1742-6596/1618/6/062042>
- Mattsson, N., Verendel, V., Hedenus, F., Reichenberg, L., 2021. An autopilot for energy models – Automatic generation of renewable supply curves, hourly capacity factors and hourly synthetic electricity demand for arbitrary world regions. *Energy Strategy Reviews* 33, 100606. <https://doi.org/10.1016/j.esr.2020.100606>
- Mayer, M.J., Biró, B., Szücs, B., Aszódi, A., 2023. Probabilistic modeling of future electricity systems with high renewable energy penetration using machine learning. *Applied Energy* 336, 120801. <https://doi.org/10.1016/j.apenergy.2023.120801>
- Mínguez, R., García-Bertrand, R., 2016. Robust transmission network expansion planning in energy systems: Improving computational performance. *European Journal of Operational Research* 248, 21–32. <https://doi.org/10.1016/j.ejor.2015.06.068>
- Ohlendorf, N., Schill, W.-P., 2020. Frequency and duration of low-wind-power events in Germany. *Environ. Res. Lett.* 15, 084045. <https://doi.org/10.1088/1748-9326/ab91e9>
- Otero, N., Martius, O., Allen, S., Bloomfield, H., Schaeffli, B., 2022a. Characterizing renewable energy compound events across Europe using a logistic regression-based approach. *Meteorological Applications* 29, e2089. <https://doi.org/10.1002/met.2089>
- Otero, N., Martius, O., Allen, S., Bloomfield, H., Schaeffli, B., 2022b. A copula-based assessment of renewable energy droughts across Europe. *Renewable Energy* 201, 667–677. <https://doi.org/10.1016/j.renene.2022.10.091>
- Plaga, L.S., Bertsch, V., 2022. Robust planning of a European Electricity System under climate uncertainty, in: 2022 18th International Conference on the European Energy Market (EEM). Presented at the 2022 18th International Conference on the European Energy Market (EEM), pp. 1–8. <https://doi.org/10.1109/EEM54602.2022.9921057>
- Raynaud, D., Hingray, B., François, B., Creutin, J.D., 2018. Energy droughts from variable renewable energy sources in European climates. *Renewable Energy* 125, 578–589. <https://doi.org/10.1016/j.renene.2018.02.130>
- Reichenberg, L., Hedenus, F., Odenberger, M., Johnsson, F., 2018. The marginal system LCOE of variable renewables – Evaluating high penetration levels of wind and solar in Europe. *Energy* 152, 914–924. <https://doi.org/10.1016/j.energy.2018.02.061>
- Riepin, I., Schmidt, M., Baringo, L., Musgens, F., 2021. European Gas Infrastructure Expansion Planning: An Adaptive Robust Optimization Approach. *Optimization Online*.
- Rogelj, J., Luderer, G., Pietzcker, R.C., Kriegler, E., Schaeffer, M., Krey, V., Riahi, K., 2015. Energy system transformations for limiting end-of-century warming to below 1.5 °C. *Nature Clim Change* 5, 519–527. <https://doi.org/10.1038/nclimate2572>
- Roldán, C., García-Bertrand, R., Mínguez, R., 2020. Robust transmission expansion planning with uncertain generations and loads using full probabilistic information. *Electric Power Systems Research* 189, 106793. <https://doi.org/10.1016/j.epr.2020.106793>
- Roldán, C., Mínguez, R., García-Bertrand, R., Arroyo, J.M., 2019. Robust Transmission Network Expansion Planning Under Correlated Uncertainty. *IEEE Trans. Power Syst.* 34, 2071–2082. <https://doi.org/10.1109/TPWRS.2018.2889032>

- Roldán, C., Sánchez de la Nieta, A.A., García-Bertrand, R., Mínguez, R., 2018. Robust dynamic transmission and renewable generation expansion planning: Walking towards sustainable systems. *International Journal of Electrical Power & Energy Systems* 96, 52–63. <https://doi.org/10.1016/j.ijepes.2017.09.021>
- Ruhnau, O., Qvist, S., 2022. Storage requirements in a 100% renewable electricity system: extreme events and inter-annual variability. *Environmental Research Letters* 17, 044018. <https://doi.org/10.1088/1748-9326/ac4dc8>
- Schlachtberger, D.P., Brown, T., Schramm, S., Greiner, M., 2017. The benefits of cooperation in a highly renewable European electricity network. *Energy* 134, 469–481. <https://doi.org/10.1016/j.energy.2017.06.004>
- Seljom, P., Kvalbein, L., Hellemo, L., Kaut, M., Ortiz, M.M., 2021. Stochastic modelling of variable renewables in long-term energy models: Dataset, scenario generation & quality of results. *Energy* 236, 121415. <https://doi.org/10.1016/j.energy.2021.121415>
- Wiel, K.V.D., Bloomfield, H.C., Lee, R.W., Stoop, L.P., Blackport, R., Screen, J.A., Selten, F.M., 2019. The influence of weather regimes on European renewable energy production and demand. *Environmental Research Letters* 14. <https://doi.org/10.1088/1748-9326/ab38d3>
- Yue, X., Pye, S., DeCarolis, J., Li, F.G.N., Rogan, F., Gallachóir, B.Ó., 2018. A review of approaches to uncertainty assessment in energy system optimization models. *Energy Strategy Reviews* 21, 204–217. <https://doi.org/10.1016/j.esr.2018.06.003>
- Zakaria, A., Ismail, F.B., Lipu, M.S.H., Hannan, M.A., 2020. Uncertainty models for stochastic optimization in renewable energy applications. *Renewable Energy* 145, 1543–1571. <https://doi.org/10.1016/j.renene.2019.07.081>
- Zerrahn, A., Schill, W.-P., Kemfert, C., 2018. On the economics of electrical storage for variable renewable energy sources. *European Economic Review* 108, 259–279. <https://doi.org/10.1016/j.euroecorev.2018.07.004>
- Zhang, X., Conejo, A.J., 2018. Robust Transmission Expansion Planning Representing Long- and Short-Term Uncertainty. *IEEE Trans. Power Syst.* 33, 1329–1338. <https://doi.org/10.1109/TPWRS.2017.2717944>

## APPENDIX A

### Overview of the system, the cost and technology data

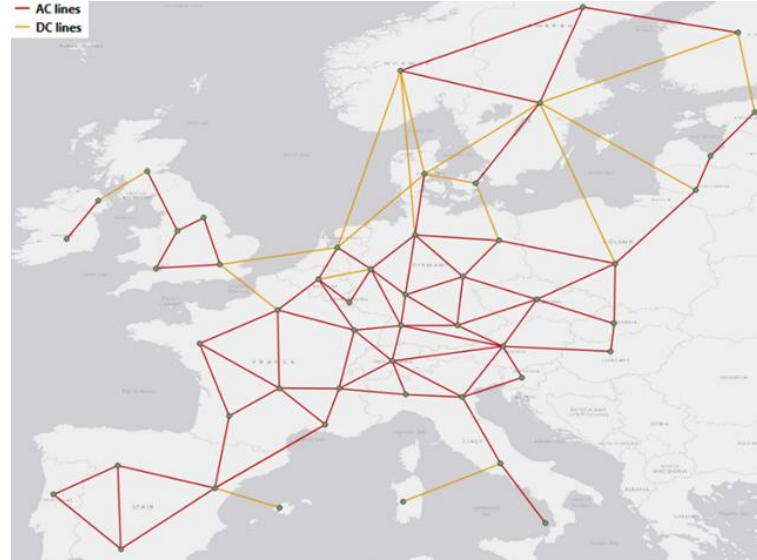


Fig. 10. Map of clustered EU high-voltage electricity system – own illustration.

Table 4: Load shedding costs

Load shedding			
Parameter	Value	Parameter	Value
$f^{L1}$	5%	$sc_n^{LS1}$	1.000 EUR/MWh
$f^{L2}$	15%	$sc_n^{LS2}$	3.000 EUR/MWh
$f^{L3}$	80%	$sc_n^{LS3}$	12.000 EUR/MWh

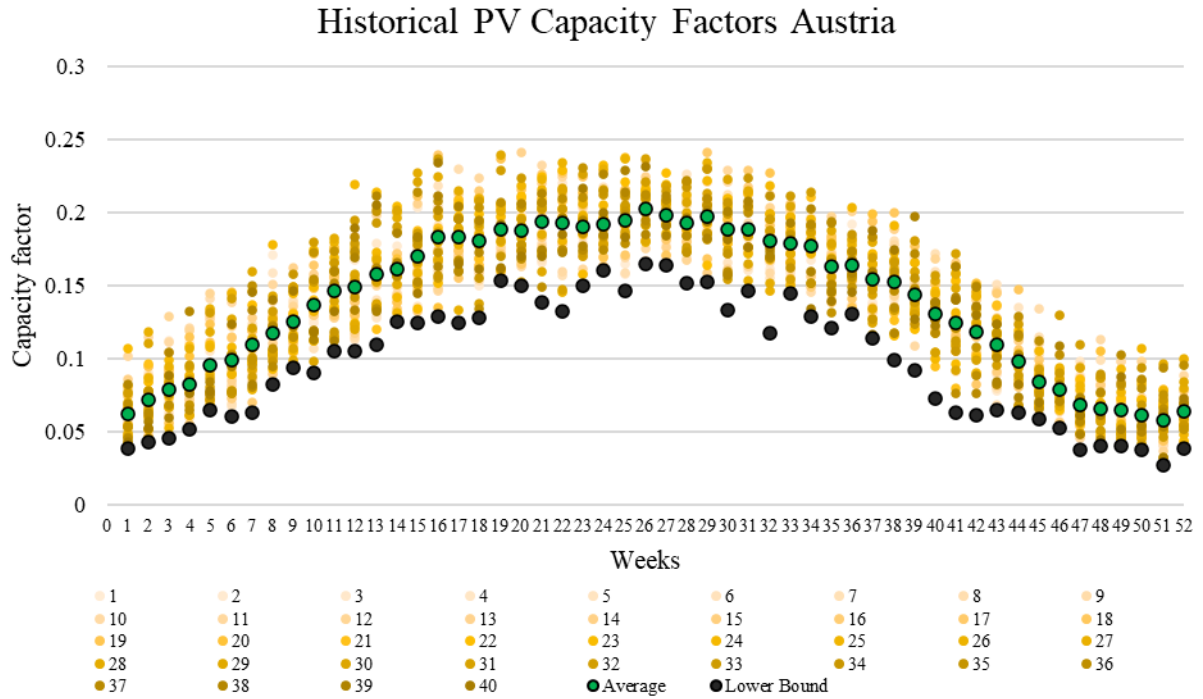
Table 5: Technology data

Technology	Lifetime in years	Interest Rate	Overnight costs	Fixed OM costs	Fuel Costs	Efficiency	Data Source
Onshore Wind	30	7.5%	963 EUR/kW	9.63 EUR/kW/y	-	-	Danish Energy Agency
Offshore Wind	30	9.3%	1380 EUR/kW	13.80 EUR/kW/y	-	-	Danish Energy Agency
Solar PV	35	6.9%	370 EUR/kW	7.40 EUR/kW/y	-	-	Danish Energy Agency
Battery Inverter	10	6.0%	60.0 EUR/kW	0.6 EUR/kW/y	-	96%	Danish Energy Agency

Battery Storage	30	6.0%	75 EUR/kWh	0.6 EUR/kWh/y	-	-	Danish Energy Agency
Electrolyzer	25	8.0%	350 EUR/kW	14 EUR/kW/y	-	70%	Danish Energy Agency
H <sub>2</sub> Storage Tank	30	8.0%	21 EUR/kWh	0.5 EUR/kWh/y	-	-	Danish Energy Agency
H <sub>2</sub> -fired OCGT	25	8.0%	411 EUR/kW	8.7 EUR/kW/y	-	43%	Danish Energy Agency
AC Transmission	40	6.0%	700-2500 EUR/MW/km	-	-	-	NEP 2023 (1)-
DC Transmission	40	6.0%	2500-5500 EUR/MW/km	-	-	-	NEP 2023 (1)-
Biomass	60	-	-	80 EUR/kW/y	4.5 EUR/MWh th	47 %	DIW (2)
Nuclear	60	-	-	100 EUR/kW/y	3 EUR/MWh th	33 %	DIW (2)
Run of River	-	-	-	35 EUR/kW/y	-	-	DIW (2), IEA
Pumping Storage	-	-	-	45 EUR/kW/y	-	-	DIW (2), IEA
Reservoir	-	-	-	40 EUR/kW/y	-	-	DIW (2), IEA

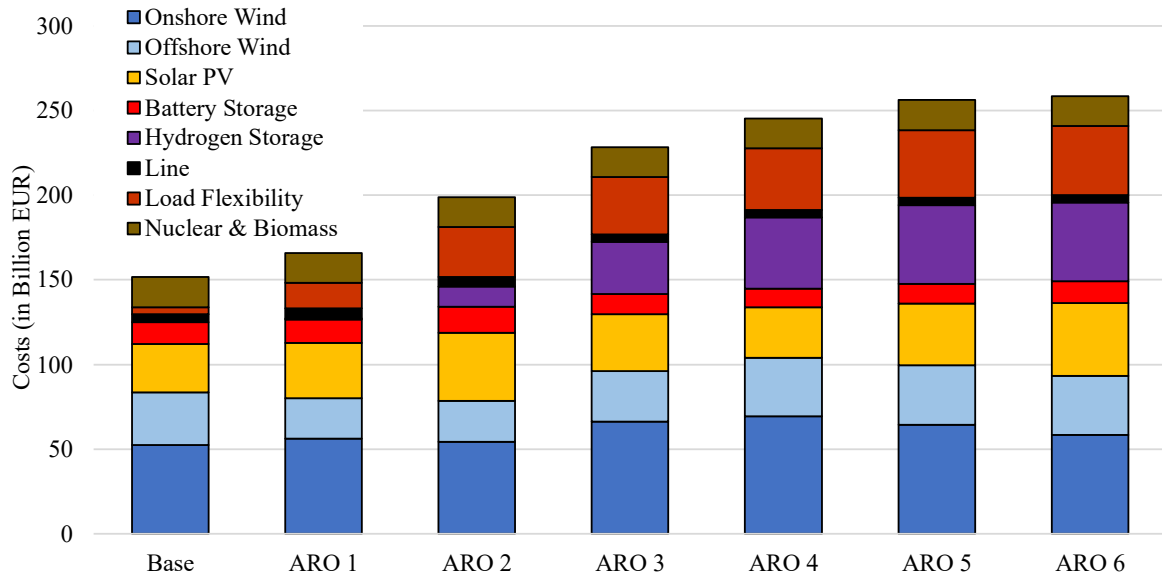
- (1) 50Hertz Transmission GmbH, Amprion GmbH, TenneT TSO GmbH & TransnetBW GmbH. (2023). Netzentwicklungsplan Strom 2037/2045 (2023): [https://www.netzentwicklungsplan.de/sites/default/files/2023-03/230321\\_NEP\\_Kostenschaetzung\\_NEP2037\\_2045\\_V2023\\_1.Entwurf.pdf](https://www.netzentwicklungsplan.de/sites/default/files/2023-03/230321_NEP_Kostenschaetzung_NEP2037_2045_V2023_1.Entwurf.pdf)
- (2) : DIW (2013): Current and prospective costs of electricity generation until 2050, [https://www.diw.de/documents/publikationen/73/diw\\_01.c.424566.de/diw\\_datadoc\\_2013-068.pdf](https://www.diw.de/documents/publikationen/73/diw_01.c.424566.de/diw_datadoc_2013-068.pdf)

## APPENDIX B



**Figure 11:** Averaged weekly solar PV capacity factors in Austria, with average weeks in green and lower bounds in black

## APPENDIX C



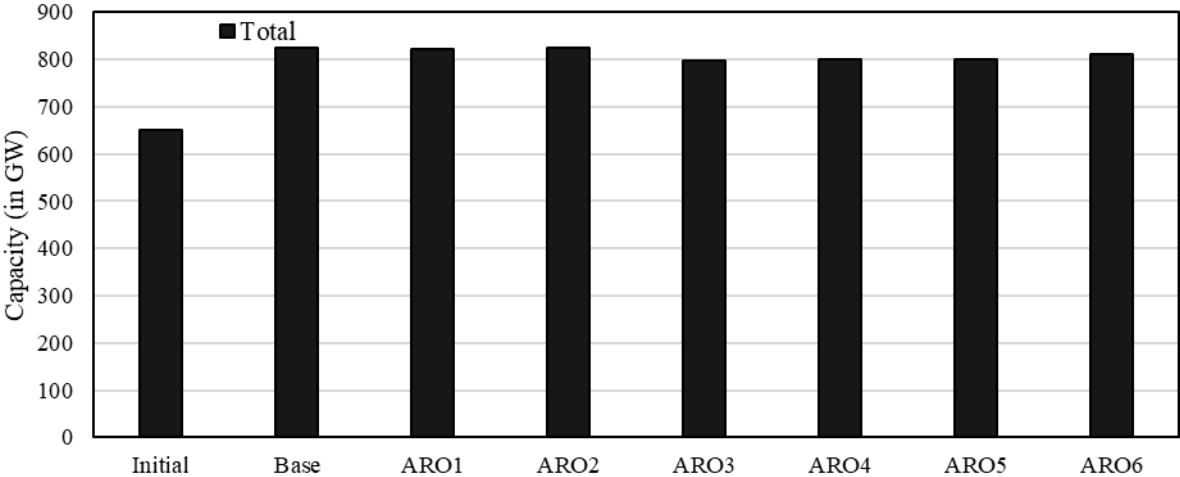
**Figure 12.** Scenario specific investments and operation costs.

Figure 12 shows the costs per scenario differentiated by generation, storage and transmission technology. As we are analyzing a carbon neutral future electricity system, the majority of the costs originate from investments in renewable generation technologies. In the base scenario (left column), wind onshore is the preferred investment, with total investment over Europe amounting to around € 50 bn. Wind offshore and solar PV follow with costs of around € 30 bn each. About € 10 bn is invested in battery storage, smaller amounts in line extensions, biomass, and nuclear operation. The base scenario does not invest in long term hydrogen storage technologies. Increasing the uncertainty budget, i.e. moving from ARO1 to ARO6 in the graph, we

can now deduce which technologies are covering the low wind and solar availabilities. Up to ARO3, the total installed capacity of RES (onshore wind, offshore wind and solar) increases. Additional capacity (MW) thus compensates for reduced availability (MWh per MW). Furthermore, investment shifts to regions which are not affected by reduced renewable availability. From ARO3 to ARO6, aggregated RES capacity remains relatively constant because increasingly more regions are affected by reduced availability. This is because expanding or reallocating renewable capacity becomes less effective in mitigating the impact. Instead, the model prioritizes the increasing use of load shedding and invests in seasonal hydrogen storage. In contrast, the share of battery storage remains almost constant from the ARO3 scenario, because it cannot contribute to shift energy beyond the daily balancing use of residual loads. The same applies to grid expansion, although at significantly lower investment levels.

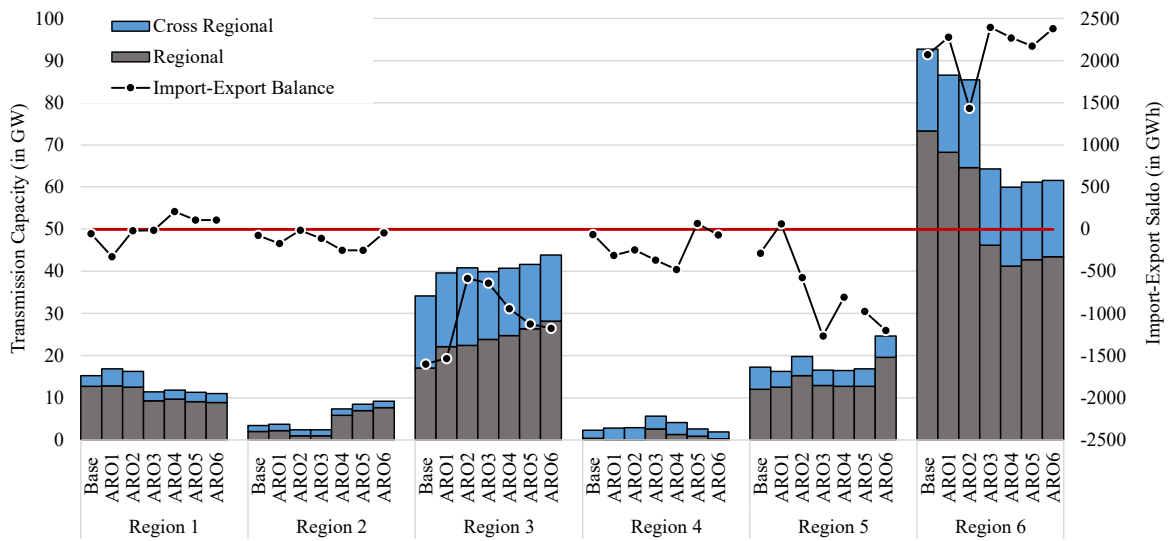
## APPENDIX D

Figure 13 plots the total transmission capacity from the initial level and for each scenario. The figure shows that in all scenarios, lines are expanded. However, in scenarios Base, ARO1 and ARO2 the expansion is at a slightly higher level as in the ARO3, ARO4, ARO5 and ARO6 scenario.



**Figure 13:** Scenario Specific Transmission Capacity Compared to Initial Capacity

Figure 14 below plots the expanded capacity for each region differentiated between the cross regional capacity and the regional (internal) transmission capacity. Additionally, it presents the import-export balance of the individual regions during the extreme event period. The figure shows that the slightly lower total transmission capacity in the ARO3-ARO6 scenarios originates from the reduced internal transmission line expansion in Region 6. Furthermore, the figure reveals that most cross-border capacity is built in Region 3 and Region 6. This is in line with the corresponding energy exchange between these regions, where Region 3 is a clear exporter and Region 6 a clear importer during all scenarios as indicated by Figure 7.



**Figure 14: Transmission capacity expansion and import-export balance during extreme event period.**

The dominating importing region throughout all scenarios is Region 6. This result is driven by two factors. The renewable availability on the one hand, and the demand centers on the other hand. Region 6 has the highest electricity demand and comparably poor renewable generation potentials compared to the other regions. Furthermore, the share of the firm capacity (exogenous hydro, biomass, and nuclear power), is the smallest compared to the overall demand. This is leading to a system layout, where Region 6 imports cheaper renewable electricity generated in neighboring regions with a better renewable potential such as Region 1, Region 3, and Region 5.

We also find that depending on the modeled extreme event, Region 6 is influencing the capacity and generation mix in its neighboring regions. For example, while Region 3 is utilizing offshore wind in the Base scenario, it switches to onshore wind generation in the ARO scenarios. In contrast, Region 6 builds more offshore wind capacity. The system seeks to minimize the distance between generation and demand centers: onshore wind is now prioritized in Region 3 due to its proximity to Region 6, while offshore wind is favored in Region 6 because, even during low wind availability events, offshore wind has greater generation potential than onshore wind.

## APPENDIX E

